Hydridorhodathiaboranes: Synthesis, Characterization and Reactivity

Álvaro Álvarez,[†] Beatriz Calvo,[†] Ramón Macías,*[†] Fernando J. Lahoz[†] and Luis A. Oro[†‡]

[†]Instituto de Síntesis Química y Catálisis Homogénea (ISQCH), Universidad de Zaragoza-Consejo Superior de Investigaciones Científicas, 50009-Zaragoza, Spain.

[‡]Center of Research Excellence in Petroleum Refining and Petrochemicals, King Fahd University of Petroleum and Minerals (KFUPM), Dhahran 31261, Saudi Arabia

E-mail: rmacias@unizar.es

July 6, 2014

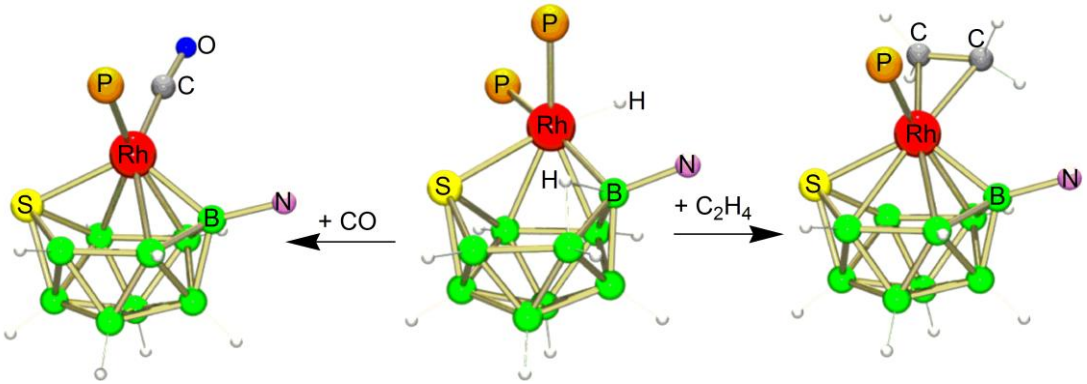

ABSTRACT

The reaction between pyridine and [8,8-$(PPh_3)_2$-*nido*-8,7-$RhSB_9H_{10}$] (**1**) has given the opportunity to synthesize a new family of 11-vertex hydridorhodathiaboranes that feature boron-bound N-heterocyclic ligands. To explore the scope of this reaction, **1** has been treated with the methylpyridine isomers (picolines), 2-Me-NC_5H_4, 3-Me-NC_5H_4 and 4-Me-NC_5H_4 affording picoline-ligated clusters, [8,8,8-(H)$(PPh_3)_2$-9-(L)-*nido*-8,7-$RhSB_9H_9$], where L = 2-Me-NC_5H_4 (**3**), 3-Me-NC_5H_4 (**4**) or 4-Me-NC_5H_4 (**5**). Thermal treatment of these *nido*-clusters leads to dehydrogenation and the formation of *isonido* / *closo*-[1,1-$(PPh_3)_2$-3-(L)-1,2-$RhSB_9H_8$] (**9**, **10**, **11**). Compounds **3-5** react with ethylene to form [1,1-(η^2-C_2H_4)(PPh_3)-3-(L)-1,2-$RhSB_9H_8$] (**13**, **14**, **15**). Similarly, treatment of **3-5** with carbon monoxide produces [1,1-(CO)(PPh_3)-3-(L)-1,2-$RhSB_9H_8$] (**17**, **18**, **19**). These series of η^2-C_2H_4- and CO-ligated 11-vertex *isonido* / *closo*-rhodathiaboranes result from the substitution of one PPh_3 ligand by ethylene or CO together with H_2 loss and a concomitant *nido*-to-*closo* / *isonido*-cluster structural transformation. The reactivity of **3-5** with propene, 1-hexene and cyclohexene in a hydrogen atmosphere is also reported and compared with the reactivity of the pyridine-ligated analogue, [8,8,8-(H)$(PPh_3)_2$-9-(NC_5H_5)-*nido*-8,7-$RhSB_9H_9$] (**2**). Low temperature NMR studies have allowed the characterization of intermediates which undergo inter- and intramolecular exchange processes, depending on the nature of the N-heterocyclic ligand. The CO ligand enhances the non-rigidity of the cluster, opening mechanisms of H_2 loss from the clusters.

MANUSCRIPT TEXT

Introduction

The reactivity of metallacarboranes with organic molecules to give polyhedral clusters that feature metal-carbon bonds has been well studied.[1] In contrast, the organometallic chemistry of metallaboranes and metallaheteroboranes (containing p-block elements other than carbon in the cluster framework) has been less well developed.[2] There is a great potential for novel chemistry in this area that may be developed by a combination of the (oxidative and coordinative) flexibility of transition metal centres together with the capability of boron-based clusters to exhibit redox flexibility in their classical *closo*-*nido*-*arachno*-*hypho* structural transformation.[3] In other words, the synergic cooperation between a metal centre and a (hetero)borane fragment can open new opportunities for bond activation and catalysis.

In the context of organometallic chemistry and catalysis based on metallaheteroboranes, we have focused our work on the 11-vertex rhodathiaborane, [8,8-$(PPh_3)_2$-*nido*-8,7-$RhSB_9H_{10}$] (**1**).[4] This polyhedral compound exhibits two principal points of reactivity: the metal centre and an adjacent B-H unit on the pentagonal face (Scheme 1). Reactions with monodentate phosphines led to the formation of metal-ligand-substitution products, [8,8-$(PR_3)(PPh_3)$-*nido*-8,7-$RhSB_9H_{10}$], as well as compounds resulting from the substitution of the PPh_3 ligands and the addition of a third phosphine at the metal centre, [8,8,8-$(PR_3)_3$-*nido*-8,7-$RhSB_9H_{10}$] (Scheme 1).[5]

Alternatively, the treatment of **1** with pyridine affords a hydridorhodathiaborane, [8,8,8-$(H)(PPh_3)_2$-9-(NC_5H_5)-*nido*-8,7-$RhSB_9H_9$] (**2**), in which the pyridine ligand binds to boron-9 adjacent to the metal on the pentagonal face (Scheme 1).[6]

The *bis*-PPh_3-ligated 11-vertex *nido*-rhodathiaborane, **1**, also undergoes substitution reactions with 1,3-dimethylimidazol-2-ylidene, IMe, giving a mixture that contains the products of monosubstitution and disubstitution, [8,8-(PPh_3)(IMe)-*nido*-8,7-$RhSB_9H_{10}$] and [8,8-$(IMe)_2$-*nido*-8,7-$RhSB_9H_{10}$] (Scheme 1).[7] The treatment of the monosubstituted carbene-ligated *nido*-

rhodathiaborane with pyridine affords a new *isonido*-cluster, [1,1-(IMe)(PPh_3)-3-(NC_5H_5)-*isonido*-8,7-$RhSB_9H_8$], formed by pyridine-cage substitution and dihydrogen loss. Interestingly, the *bis*-carbene-ligated analogue does not react with pyridine.

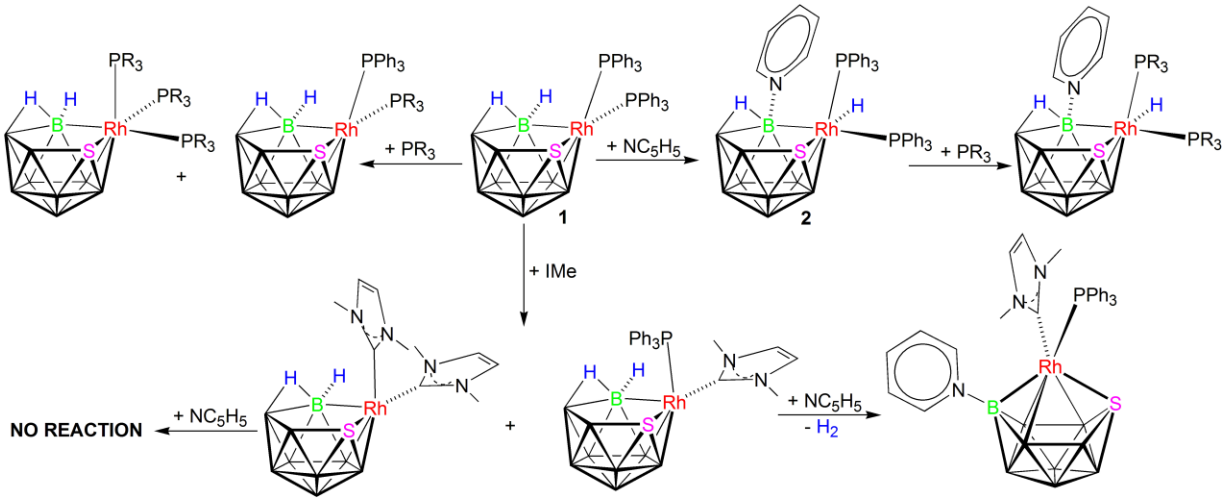

Scheme 1 Reactivity of compounds **1** and **2** with Lewis bases: systematic cluster tailoring

These results demonstrate that compounds **1** and **2** are versatile clusters that can be easily prepared and systematically modified at the rhodium centre by substitutional chemistry. The fact that the *exo*-polyhedral ligands play a crucial role in the reactivity of these clusters is clearly demonstrated by the different outcomes of the reactions with pyridine.

Recently, we have reported that the treatment of *nido*-hydridorhodathiaboranes, [8,8,8-(H)(PR_3)$_2$-9-(NC_5H_5)-8,7-$RhSB_9H_9$], and *closo* / *isonido*-clusters, [1,1-(PR_3)$_2$-3-(NC_5H_5)-1,2-$RhSB_9H_8$], with triflic acid yield the corresponding cationic rhodathiaboranes, [8,8,8-(H)(PR_3)$_2$-9-(NC_5H_5)-*nido*-8,7-$RhSB_9H_{10}]^+$ and [1,1-(PR_3)$_2$-3-(NC_5H_5)-*isonido*-1,2-$RhSB_9H_8]^+$.[8] These polyhedral cations show a remarkable stereochemical non-rigidity that is the key to their reactivity.

Overall, this family of neutral and cationic 11-vertex rhodathiaboranes has revealed a rich chemistry that embraces: *(i) nido*-to-*closo* dehydrogenations,[9] *(ii)* dihydrogen promoted *closo*-to-

nido transformations[6b,7], *(iii)* oxidative addition of *sp* C–H bonds,[10] *(iv)* proton-assisted H_2 activation[11] and *(v)* catalysis of hydrogenation and isomerization of olefins.[6b]

In these reactions, the clusters exhibit metal-borane collaboration through structural transformations that lead to metal-ligand hapticity changes. In other words, these NC_5H_5-ligated rhodathiaboranes combine the flexibility of the $\{Rh(PPh_3)_2\}$-centre with the capability of the 11-vertex $\{RhSB_9\}$-cage to exhibit redox flexibility through *closo*-*nido* structural transformations. This metal / borane synergy has resulted in the development of new stoichiometric cycles.[6,12]

Based on the results summarized above, we logically aimed to change the pyridine substituent at the boron vertices. Herein, we report the reactions of the parent rhodathiaborane, **1**, with the methylpyridine isomers (picolines), 2-Me-NC_5H_4, 3-Me-NC_5H_4 and 4-Me-NC_5H_4. The new picoline-ligated clusters are compared with their pyridine counterparts, in order to find trends and differences within this unique series of polyhedral clusters. In addition, the reactivity of these rhodathiaboranes has been studied with as focus on hydrogen loss, and on their reactions with ethylene and CO.

Results and Discussion

Synthesis and characterization of picoline-ligated 11-vertex rhodathiaboranes

Reaction of compound **1** with excess of 2-picoline afforded a mixture containing the hydridorhodathiaboranes, [8,8,8-(H)$(PPh_3)_2$-9-(2-Me-NC_5H_4)-*nido*-8,7-$RhSB_9H_9$] (**3**) and [1,1-$(PPh_3)_2$-3-(2-Me-NC_5H_4)-*isonido*-1,2-$RhSB_9H_8$]. The latter compound is the result of 2-picoline-cage substitution and dihydrogen loss (*vide infra*), affording a cluster with a *closo* / *isonido*-electron count.

Under the same conditions, the reaction of **1** with 3- or 4-picoline afforded good yields of air-stable red solids that were characterized as the hydridorhodathiaboranes, [8,8,8-(H)$(PPh_3)_2$-9-(3-Me-NC_5H_4)-*nido*-8,7-$RhSB_9H_9$] (**4**) and [8,8,8-(H)$(PPh_3)_2$-9-(4-Me-NC_5H_4)-*nido*-8,7-$RhSB_9H_9$] (**5**); mirroring the results previously obtained with pyridine (Scheme 2).[6]

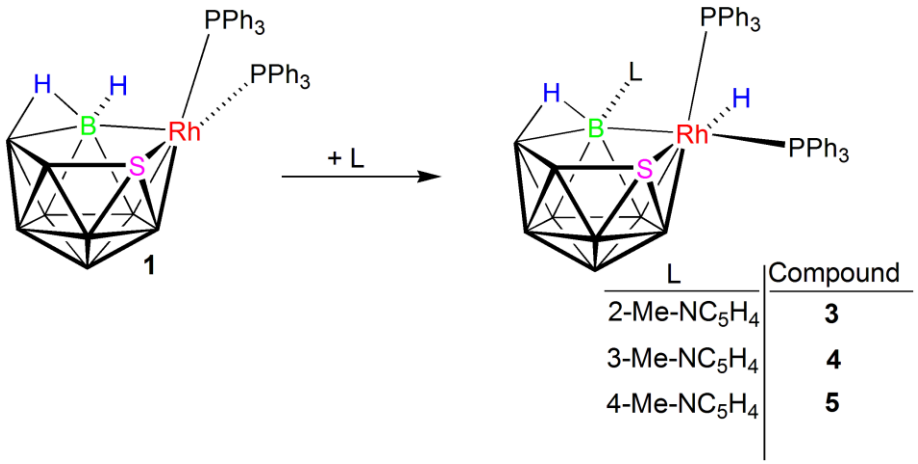

L	Compound
2-Me-NC_5H_4	**3**
3-Me-NC_5H_4	**4**
4-Me-NC_5H_4	**5**

Scheme 2 Synthesis of hydridorhodathiaboranes.

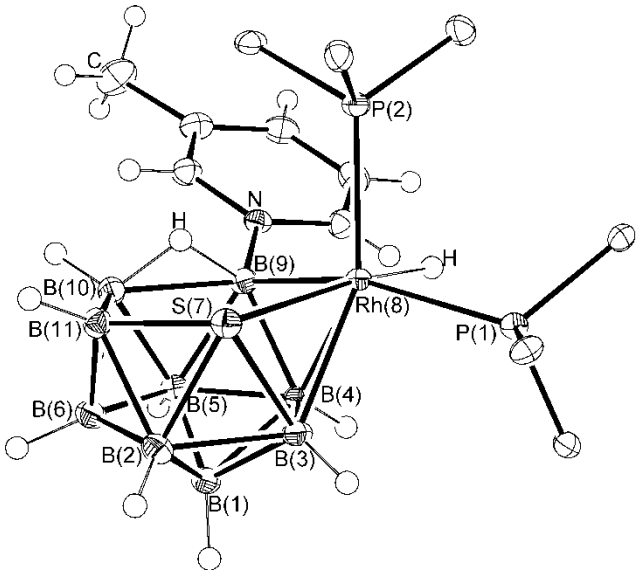

Figure 1 Molecular structure of **4**. Only the *ipso*-carbon atoms on the phenyl groups are included to aid clarity. Ellipsoids are shown at 50 % probability levels.

The three new hydridorhodathiaboranes, **3-5**, have been characterized by multielement NMR spectroscopy. In addition, the molecular structures of the 3- and 4-picoline-ligated compounds have been determined by X-ray diffraction analysis. The structures are based on an 11-vertex *nido*-{$RhSB_9$} skeleton that can be formally derived from an icosahedron by the removal of a vertex. The pentagonal face is made up by a {Rh(H)(PPh_3)} group, a sulfur vertex, two BH units

and a boron vertex substituted by an N-heterocyclic ligand (Figure 1). In addition, there is a bridging hydrogen atom along the B(9)-B(10) edge. The same structural motifs are found in the pyridine-ligated analogues, [8,8,8-(H)$(PR_3)_2$-9-(NC_5H_5)-*nido*-8,7-$RhSB_9H_9$], where PR_3 = PPh_3 (**2**) or $PMePh_2$ (**6**) (Table 1).[5-6,9] Compounds **2**-**6** are 13 skeletal electron pair clusters (sep) that conform to Wade's rules.[3a] This fact contrasts with the precursor **1** that has 12 sep, typical of a *closo* / *isonido* cage, but exhibits an 11-vertex *nido*-structure. This discrepancy between skeletal electron pairs and structure has been dealt with previously in detail.[13]

Table 1 gathers selected distances and angles for compounds **2**, **4**, **5** and **6**. Overall, there are no substantial differences between intramolecular distances and angles in these series of hydridorhodathiaboranes. It is noteworthy, however, that the 3-picoline derivative, **4**, exhibits the longest Rh–P distance at 2.3752(8) Å, perhaps due to steric interactions between the methyl group at the position 3 in N-heterocyclic ring and the bulky PPh_3 ligands. In all the clusters but **5**, the longest Rh–P distance corresponds to the phosphine ligand that is *trans* to boron-9, substituted with the pyridinic ligand, suggesting a stronger structural *trans*-influence than the B(3)–B(4) edge to which the other phosphine, P(2), lies *trans*. The shorter Rh–P distances found in the *bis*-$PMePh_2$ derivative, **6**, agree well with the fact that methyldiphenylphosphine is a better σ-donor ligand than PPh_3.

It is well known that the boron vertices of metal-face-bound carborane ligands have a larger *trans* influence than the cage carbon atoms.[14] This fact is important because implies that the most stable metal-to-carborane *exo*-polyhedral ligand orientation is that in which the strongest structural *trans*-effect ligands on the metal lie effectively *trans* to the carbon atoms. This may be extended to metallathiaboranes where the metal-bound sulfur atom also have a lower *trans* influence than the boron atoms in the face of the metal-to-thiborane linkage. Thus, in the hydridorhodathiaboranes **2**-**6**, the hydride ligand lies *trans* to the sulfur vertex. The same kind of *exo*-polyhedral ligand control has been observed in other metallathiaboranes that bear hydride

ligands.[15] Moreover, in some 11-vertex *nido*-rhodathiaboranes, it has been calculated that a metal-thiaborane interaction change from a sulfur-metal-hydride *trans*-arrangement to a boron-metal-hydride *trans*-configuration can have an energy cost as high as 12 kcal/mol.[12,16]

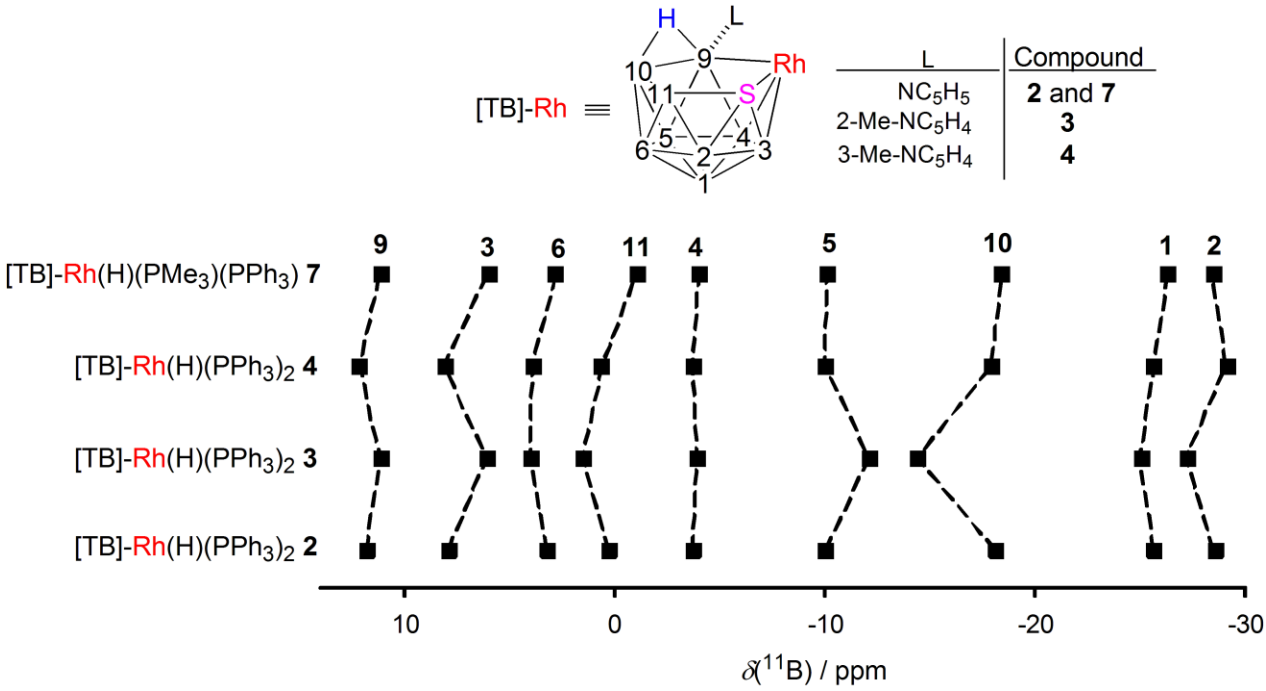

Figure 2 Representation of the ^{11}B NMR spectra of **2-4** and **7**. Hatched lines connect equivalent positions. Assignments made based on DFT-calculations.

^{11}B and ^{1}H NMR data for compounds **3-5** are listed in Table 2; and Figure 2 compares the ^{11}B spectra of the 2- and 3-picoline-ligated clusters, **3** and **4**, with those of the previously reported pyridine analogues, **2** and [8,8,8-(H)(PMe$_3$)(PPh$_3$)-9-(NC$_5$H$_5$)-*nido*-8,7-RhSB$_9$H$_9$] (**7**). These *nido*-hydridorhodathiaboranes show nine resonances in the interval between δ_B +15 to -30 ppm, in agreement with an asymmetric molecular structure in solution. The spectra between the clusters are remarkably similar, with the only noticeable deviation corresponding to the B(10) resonance of the 2-picoline derivative, which is deshielded by about 4 ppm from the general trend (Figure 2).

The ^{1}H-{^{11}B} NMR spectra of **3-5** show a broad singlet and an apparent quartet in the high-field region, assigned to the B(9)–B(10) bridging hydrogen atom and to the Rh–H hydride ligand,

respectively. Thus, these spectroscopic data can be taken as diagnostic for the formation of these 11-vertex *nido*-hydridorhodathiaboranes. In this regard, it is interesting to note that the B(9)–H–B(10) bridging proton resonance of the 2-picoline derivative (δ_H -0.95 ppm) features a significant shift towards low frequency from the mean value of δ_H -1.28 ppm that has been found in the series of picoline-ligated *nido*-clusters reported here, as well as the previously reported hydridorhodathiaborane counterparts of general formulation, [8,8,8-(H)$(PR_3)_2$-9-(NC_5H_5)-*nido*-8,7-$RhSB_9H_9$], where PR_3 = PPh_3 (**2**), $PMePh_2$ (**6**), PPh_3 and PMe_3 (**7**), $PPhMe_2$, or PPh_3 and PMe_2Ph.[9]

The lower conformational freedom of the 2-picoline substituent around the B(3)–N bond compared to the pyridine, 3- and 4-picolines may be the cause of the shift to higher frequency of the B(9)–H–B(10) bridging proton resonance.

The ^{31}P-$\{^1H\}$ spectra of **3**-**5** exhibit two doublet of doublets at low temperature, the signal at the highest frequency being significantly broader. This latter resonance broadens and shifts to low-frequency as the temperature increases, whereas the low-frequency signal moves slightly to higher frequency. This variable temperature NMR behavior is illustrated in Figure S1 for compound **5**: from low to high temperatures, the two resonances broaden and cross each other. Similar changes were first reported for the pyridine analogue **2**.[6a]

It has been proposed that the temperature-dependent broadening in the ^{31}P-$\{^1H\}$ spectra of pyridine-ligated hydridorhothiaboranes, [8,8,8-(H)$(PR_3)_2$-9-(NC_5H_5)-*nido*-$RhSB_9H_9$], may arise mainly from the effects of "thermal decoupling" on the boron nuclei,[17] together with the dissociation of the phosphine ligand *trans* to B(9).[6b,9] On this rationale, the broader peak at high frequency in this new family of 11-vertex hydrido-ligated clusters may be assigned to the phosphine ligand that is *trans* to the picoline-substituted boron vertex at the 9-position.

Studies of reactivity

Thermal and chemical cluster dehydrogenations. The hydridorhodathiaboranes, **3**-**5**, are stable in solution at room temperature. However, heating at reflux temperature in dichloromethane results in the loss of H_2, yielding the corresponding *closo* / *isonido* clusters, [1,1-$(PPh_3)_2$-3-(L)-1,2-$RhSB_9H_8$], where L = 2-Me-NC_5H_4 (**9**), 3-Me-NC_5H_4 (**10**) or 4-Me-NC_5H_4 (**11**) (Scheme 3).

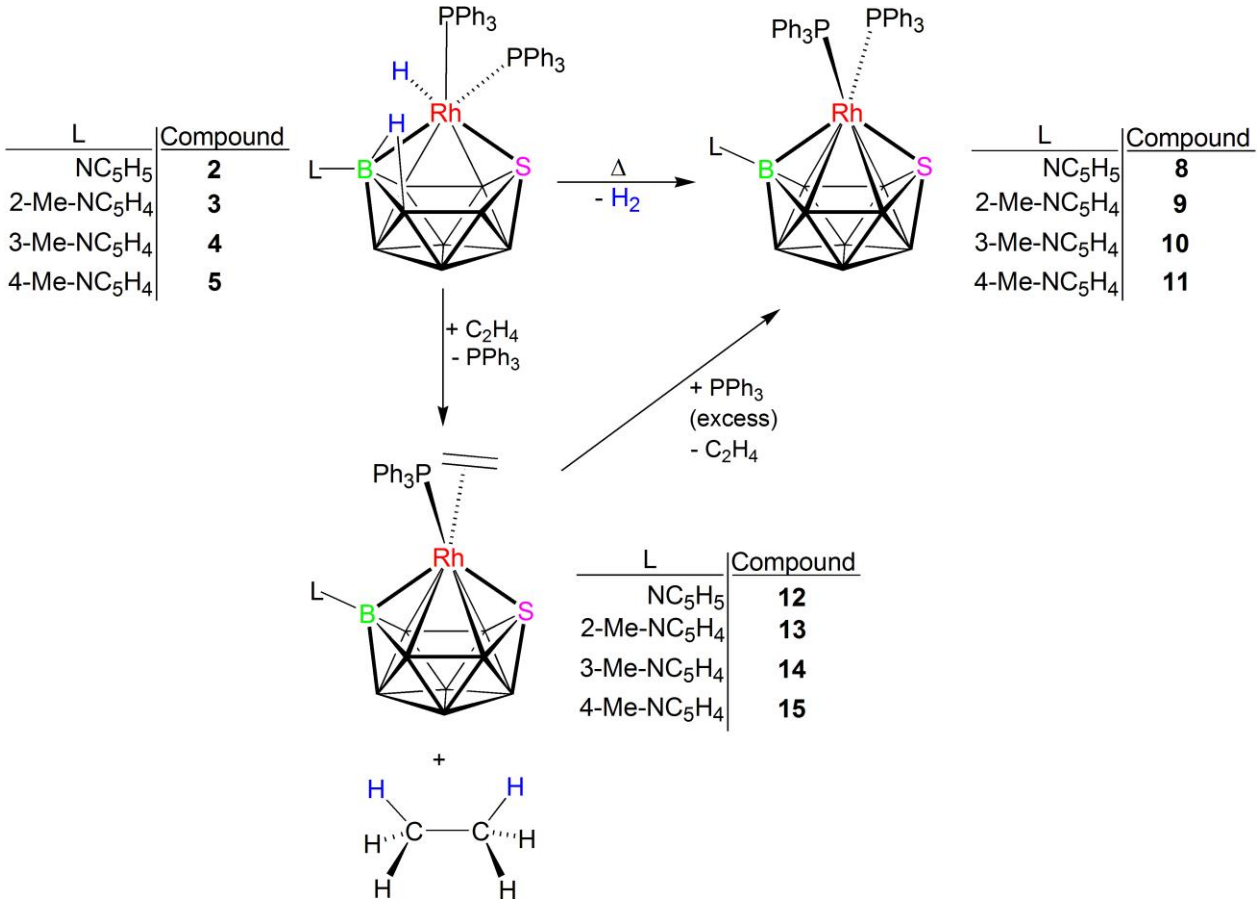

Scheme 3 Reactivity of **2**-**5**: thermal dehydrogenation, and reactions with C_2H_4.

The picoline-ligated rhodathiaboranes, **2**-**5**, react with ethylene to give the corresponding *closo* / *isonido*-clusters, [1,1-(η^2-C_2H_4)(PPh_3)-3-(L)-1,2-$RhSB_9H_8$] (**13**–**15**). In these reactions, we have also observed formation of ethane.

The η^2-C_2H_4 ligand in these 11-vertex *closo* / *isonido*-clusters is labile and it can be substituted by PPh_3 to give the corresponding *bis*-PPh_3-ligated derivatives (Scheme 3). In fact, this route is more appropriate for the synthesis of the *closo* / *isonido* compounds, **8**-**11**, than the thermal dehydrogenation of the hydride *nido*-clusters, **2**-**5**.

The reactivity of compounds **2** and **3** has been also explored with other alkenes. Thus, the pyridine-ligated cluster, **2**, reacts slowly with propylene at room temperature, and, after four days of stirring, the result is a mixture that contains propane together with the starting reagent, **2** (35%) and its dehydrogenation product, **8** (65 %). The reaction with 1-hexene, after three days, afforded 1-hexene (75%), 2-hexene (17%), 3-hexene (7%) and 1-hexane (1%). Under the same conditions, compound **2** did not react with cyclohexene.

In the case of the 2-picoline analogue, **3**, in one hour the reaction with propylene affords the *bis*-(PPh_3) *closo*-derivative, **9**, and formation of propane. Reaction with 1-hexene, after one day, gave a mixture composed of 1-hexene (63%), 2-hexene (34%), and 1-hexane (3%). Moreover, **3** reacted with cyclohexene to give 2 % of cyclohexane after one day. These results demonstrate that the 2-picoline derivative **3** is more reactive with alkenes that the pyridine analogue, **2**, and that the reaction products are the result of the hydrogenation and isomerization of the double bonds (in the case of 1-hexene).

In a similar fashion to the reactions with ethylene, the treatment of these pyridine and picoline-ligated hydridorhodathiaboranes, **2-5**, with carbon monoxide affords the products of hydrogen loss and PPh_3 substitution, [1,1-(CO)(PPh_3)-3-(L)-1,2-$RhSB_9H_8$], (**17**–**19**) (Scheme 4).[6a]

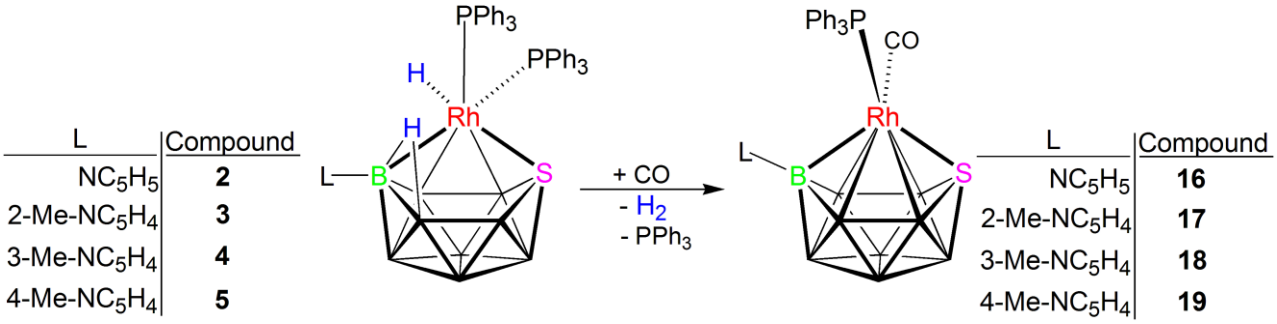

L	Compound
NC_5H_5	**2**
2-Me-NC_5H_4	**3**
3-Me-NC_5H_4	**4**
4-Me-NC_5H_4	**5**

L	Compound
NC_5H_5	**16**
2-Me-NC_5H_4	**17**
3-Me-NC_5H_4	**18**
4-Me-NC_5H_4	**19**

Scheme 4 Reactions of **2-5** with carbon monoxide

It should be note that the reactivity of the picoline-ligated hydridorhodathiaboranes, **3-5**, with carbon monoxide and with ethylene, reported here, reproduces the results previously reported for the pyridine-ligated analogue, **2**.[6b]

As we can see, thermal dehydrogenation, and reactions with CO and C_2H_4 are convenient routes to the synthesis of 11-vertex rhodathiaboranes with *closo* / *isonido*-cluster geometries, which bear different *exo*-polyhedral ligands either at the metal centre or the boron-3 vertex. Thus, these reactions broaden the scope of the substitution chemistry in this system, allowing a systematic tuning of their reactivity.

All the new 11-vertex *isonido*-clusters, **9-11**, **13-15** and **17-19**, have been characterized by NMR spectroscopy, and the data are gathered in Tables 3, 4 and 5. A comparison of the ^{11}B NMR spectra corresponding to the pyridine derivative, **8**, and the 2-picoline derivatives, **9**, **13** and **17**, is depicted in Figure 3. The patterns are very similar within this series of 11-vertex *closo* / *isonido*-clusters, suggesting that changes between the *exo*-polyheral ligands, either at the metal or at the boron vertex, do not substantially affect the overall shielding of the boron cage nuclei.

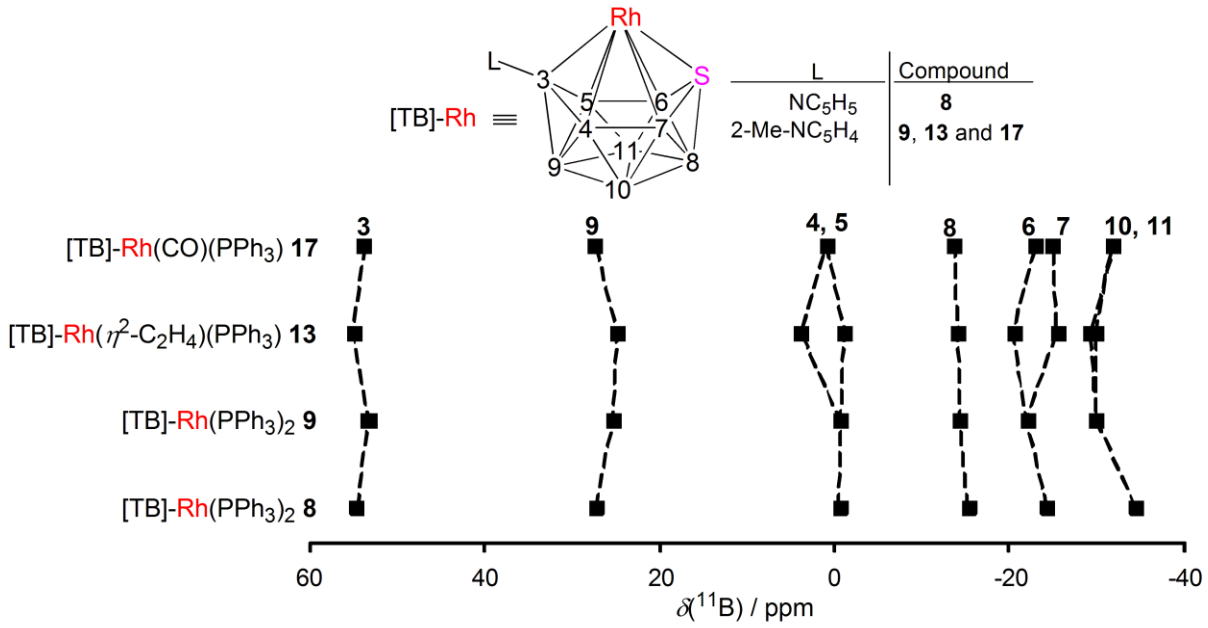

Figure 3 Diagram that represents the chemical shifts in the ^{11}B NMR spectra of **8**, **9**, **13** and **17**. Hatched lines connect equivalent positions. Assignments based on DFT GIAO calculations.

The ^{31}P-{^1H} NMR spectra of the *closo* / *isonido*-derivatives, **8-19**, show doublets at room temperature. It is of interest to note that, as the temperature decreases, the broad doublet of the 2-picoline derivative, **9**, broadens further and splits into two broad doublets. This variable-

temperature behavior demonstrates that the cluster is undergoing a fluxional process. A plausible mechanism that could rationalize this intramolecular rearrangement is a hindered rotation of the 2-pioline ligand around the N–B(3) bond, rendering the *exo*-polyhedral PPh_3 ligands at the rhodium centre nonequivalent (Scheme 5). The free energy of activation, $\Delta G^{\ddagger}_{273}$, measured at the coalesce temperature, is 12 kcal/mol.

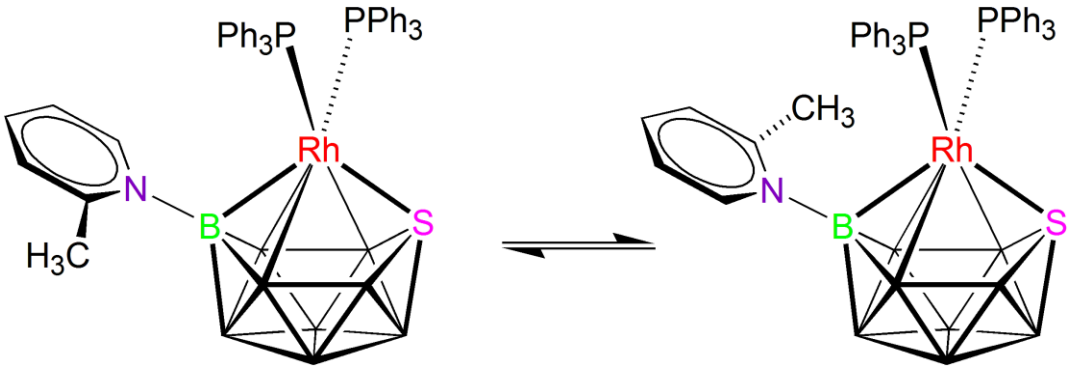

Scheme 5 Hindered rotation of the 2-picoline ligand around the B(3)–N bond in compound **9**.

Table 6 gathers the IR CO stretching frequencies of the CO-ligated *closo / isonido*-clusters, **16-19**. The frequencies are similar within the series, with the smallest value corresponding to the 3-picoline derivative. The DFT-calculated values are around 76 cm^{-1} smaller than the measured data, and they follow the experimental trend. Decreasing CO frequency is an accepted measure of increasing negative charge buildup on the metal centre. Hence, it appears that the substitution of the boron-3 with the N-heterocyclic ligands studied herein does not lead to a significant charge difference at the metal centre.

Table 6 Measured and calculated IR stretching frequencies

	$\nu_{CO}(cm^{-1})$	
Compound	ν_{exp}	ν_{calc}*
[1,1-(CO)(PPh_3)-3-(NC_5H_5)-1,2-$RhSB_9H_8$] (**16**)	1980	1903
[1,1-(CO)(PPh_3)-3-(2-Me-NC_5H_4)-1,2-$RhSB_9H_8$] (**17**)	1982	1905
[1,1-(CO)(PPh_3)-3-(3-Me-NC_5H_4)-1,2-$RhSB_9H_8$] (**18**)	1974	1898
[1,1-(CO)(PPh_3)-3-(4-Me-NC_5H_4)-1,2-$RhSB_9H_8$] (**19**)	1985	1911

*The computed carbonyl frequencies were scaled with a 0.9613 factor.[18]

The 2-picoline-ligated cluster, **9**, has been characterized by X-ray crystallography (Figure 4). Table 7 lists selected distances and angles for this derivative and, to help comparison, for the pyridine-ligated analogues, [1,1-(PR_3)-3-(NC_5H_5)-1,2-$RhSB_9H_8$], where PR_3 = PPh_3 (**8**), PMe_3 and PPh_3 (**20**), or PMe_2Ph (**21**). At first sight, the structures all look like 11-vertex *closo*-clusters based on an octadecahedron. It should be noted that the clusters exhibit long Rh(1)–B(5) distances close to 2.5 Å, which is the upper limit normally considered as bonding. In the case of compound **8**, this distance at 2.562(6) Å is outside this limit. This elongation results in the formation of a *pseudo*-square open face that is a structural feature common in *closo*-11-vertex clusters,[19] which represent intermediates along the structural continuum from *closo* to *nido*.[16,20]

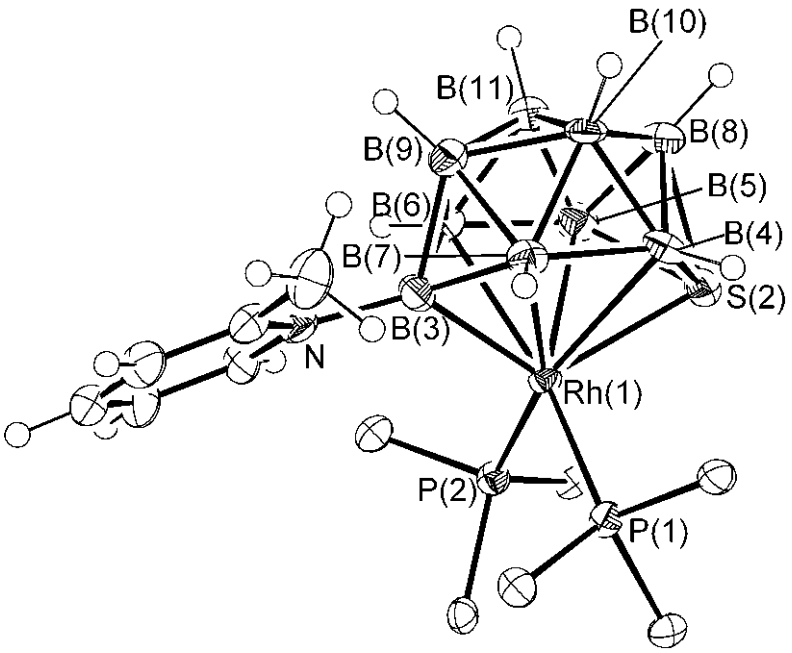

Figure 4 Molecular structure of [1,1-(PPh_3)$_2$-3-(2-Me-NC_5H_4)-*closo*-1,2-$RhSB_9H_8$] (**9**). Only the *ipso*-carbon atoms on the phenyl groups are included to aid clarity. Ellipsoids are shown at 50 % probability levels.

Reactions with CO at low temperatures. In the previous section, it was mentioned that the reaction of 11-vertex rhodathiaboranes with carbon monoxide affords the products of dihydrogen loss and the substitution of one of the PPh_3 ligands by CO. These reactions are quantitative when carried out at room temperature for periods in the order of hours. However,

short reaction times and low temperature NMR studies have allowed the characterization of intermediates that provide new insights dealing with the mechanism of hydrogen loss from these clusters. These results are, therefore, relevant to the reverse reaction: the addition of H_2 to some 11-vertex *isonido*-rhodathiaboranes.[6a,7] The following paragraphs describe these results.

Carbon monoxide was bubbled for 2 minutes through a CD_2Cl_2 solution of the 2-picoline-ligated hydridorhodathiaborane, **3**, in a 5 mm NMR tube at room temperature, and the resulting reaction mixture was then studied by variable temperature (VT) multielement NMR spectroscopy, starting at low temperatures. At -50 ºC, the ^{31}P-$\{^1H\}$ spectrum shows a sharp doublet at δ_P +35.0 ppm and a very broad peak at δ_P +33.8 ppm, together with free PPh_3 and small amounts of $O{=}PPh_3$. Interestingly, at 0 ºC, the broad signal sharpens and shifts towards higher frequency to became a doublet that overlaps the highest intensity doublet (Figure S2). The ^1H-$\{^{11}B\}$ NMR spectra at -70 and -50 ºC show three peaks in the negative region. The two broad signals at δ_H -2.93 and -4.67 ppm can be assigned to B–H–B bridging hydrogen atoms, which typically occupy positions at B–B edges on the non-triangulated open faces of boron-based clusters. The sharp doublet at δ_H -11.33 ppm corresponds to a Rh–H hydride ligand. The ^1H NMR hydride resonance broadens considerably as the temperature rises, indicating that the hydride ligand is undergoing site exchange (Figure S3). This is confirmed by a [^1H-^1H] NOESY experiment at 0 ºC that shows off-diagonal peaks of the same phase as the diagonal peak between the broad B–H–B proton signal at -2.93 ppm and the Rh–H hydride resonance (Figure 5).

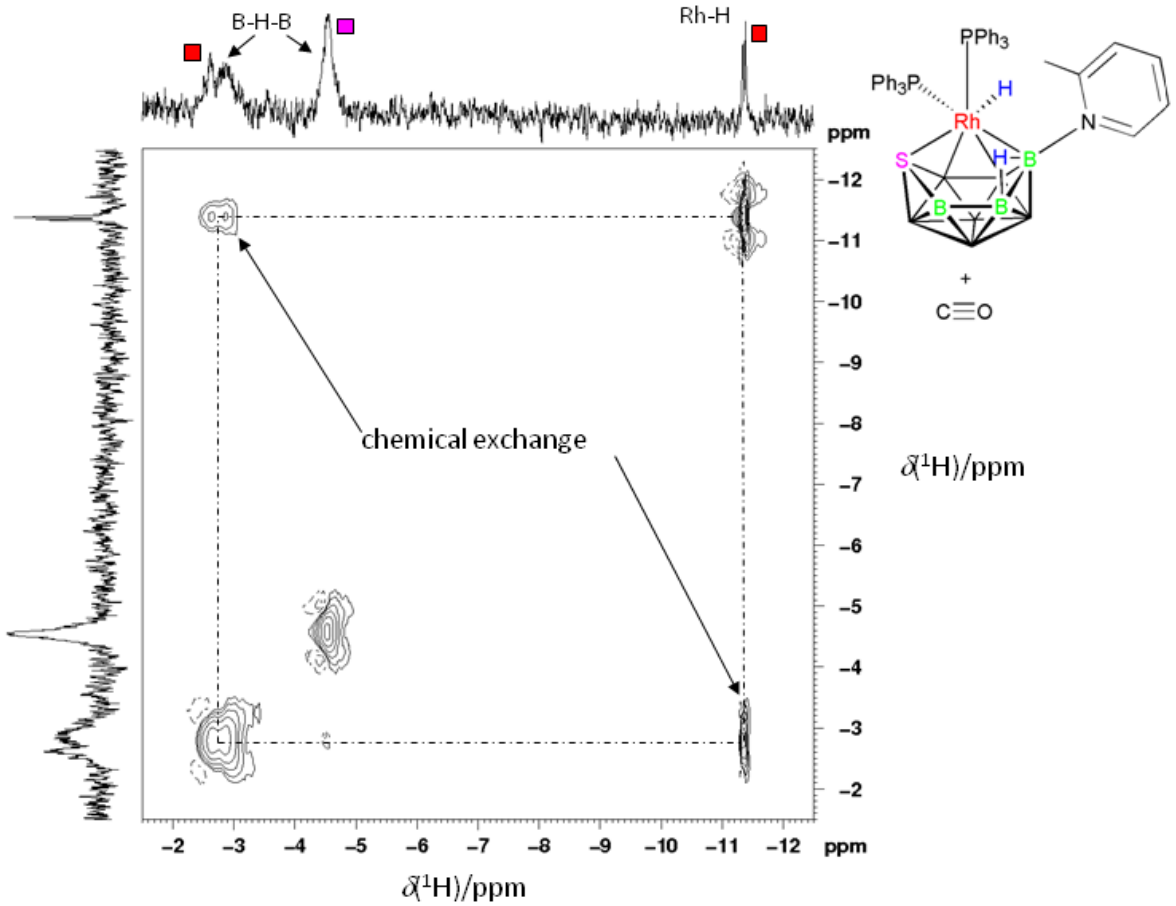

Figure 5 [^{1}H-^{1}H]-NOESY at 273 K in CD_2Cl_2 of the reaction mixture formed after the treatment of **3** with CO. The off-diagonal peaks are of the same phase as the diagonal peaks, indicating chemical exchange.

Similarly, the reaction mixtures resulting from the bubbling of CO for several minutes through CD_2Cl_2 solutions of the hydridorhodathiaboranes, **2**, **4** and **5**, at room temperature, were studied by VT NMR spectroscopy starting at low temperature. For the three systems, the ^{31}P-{^{1}H} NMR spectra at -50 °C exhibit three doublets at around +36.5, +34.5 and +29.2 ppm. In the three samples studied, the highest intensity signal corresponds to the peak close to +34 ppm, whereas the doublet at highest field exhibits the lowest intensity (Figure 6). The ^{31}P-{^{1}H} spectra showed free PPh_3, $OPPh_3$, together with different amounts of the products of H_2 loss, **8**, **10** and **11,** and the product of H_2 loss and CO-binding, **16**, **18** and **19**.

Interestingly, at higher temperatures these ^{31}P-{^{1}H} resonances (purple, red and green squares in Figures 6, S7, S8, S9 and S10) broaden and shift, suggesting that the species are undergoing processes of interconversion in solution.

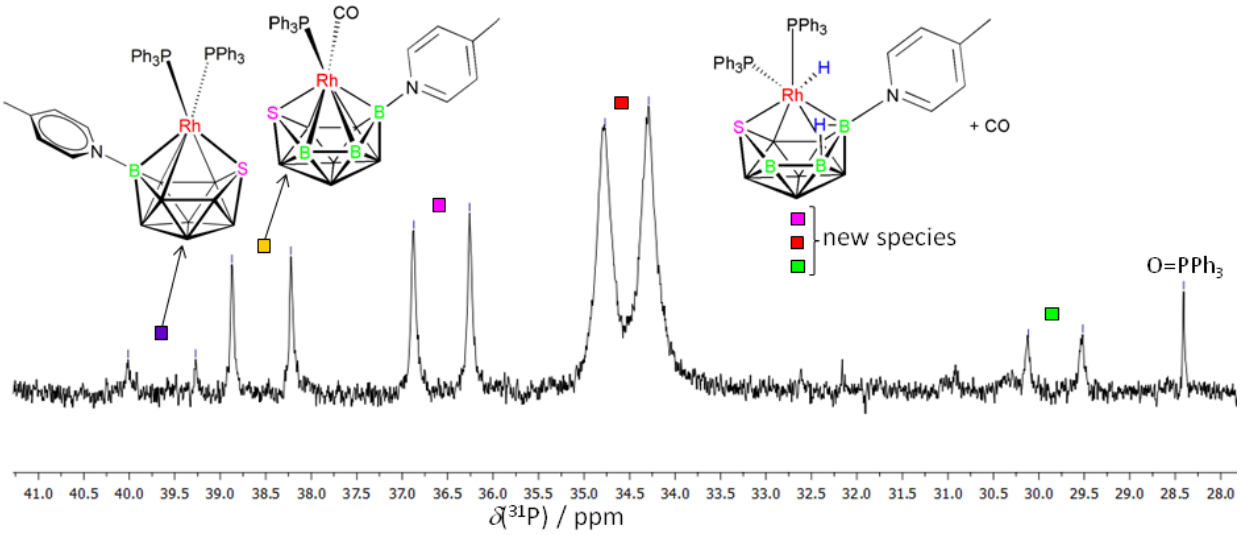

Figure 6 ^{31}P-{^{1}H} NMR spectrum in CD_2Cl_2 of compound **5** after treatment with CO at 223 K.

The ^{1}H-{^{11}B} NMR spectra of the pyridine, 3- and 4-picoline-ligated systems with CO each show two broad singlets at *ca.* δ_H -3.0 and -4.5 ppm and a sharp doublet at *ca.* -11.5 ppm (Figure 7). This pattern resembles the ^{1}H-{^{11}B} spectra discussed above for the 2-picoline system (Figure S3), and, following the same rationale, the broad resonances can therefore be assigned to B–H–B bridging hydrogen atoms and the low frequency doublet to a Rh–H hydride ligand.

It should be noted that, in the ^{1}H-{^{11}B} spectra of the pyridine, and 3- and 4-picoline ligated species, there are two new low-intensity peaks: one at around δ_H -1.7 ppm and the other at around -11.0 ppm (green squares in Figures 7, 8, S5 and S6). These signals may be attributed to a B–H–B bridging hydrogen atom and a hydride ligand of a new isomer that is not observed in the reaction with the 2-picoline-ligated derivative, **3**.

For the three systems formed upon treatment of **2**, **4** and **5**, with CO, the small intensity peaks (green squares) disappear as the temperature increases, whereas the two resonances at around δ_H -3.0 and -4.5 ppm broaden and coalesce into a broad peak (Figure 7). This VT NMR behavior clearly contrasts with the 2-picoline derivative described earlier where, as the temperature

increases, the rearrangement process involves the hydride ligand and one of the B–H–B hydrogen atoms (Figure 5 and S3).

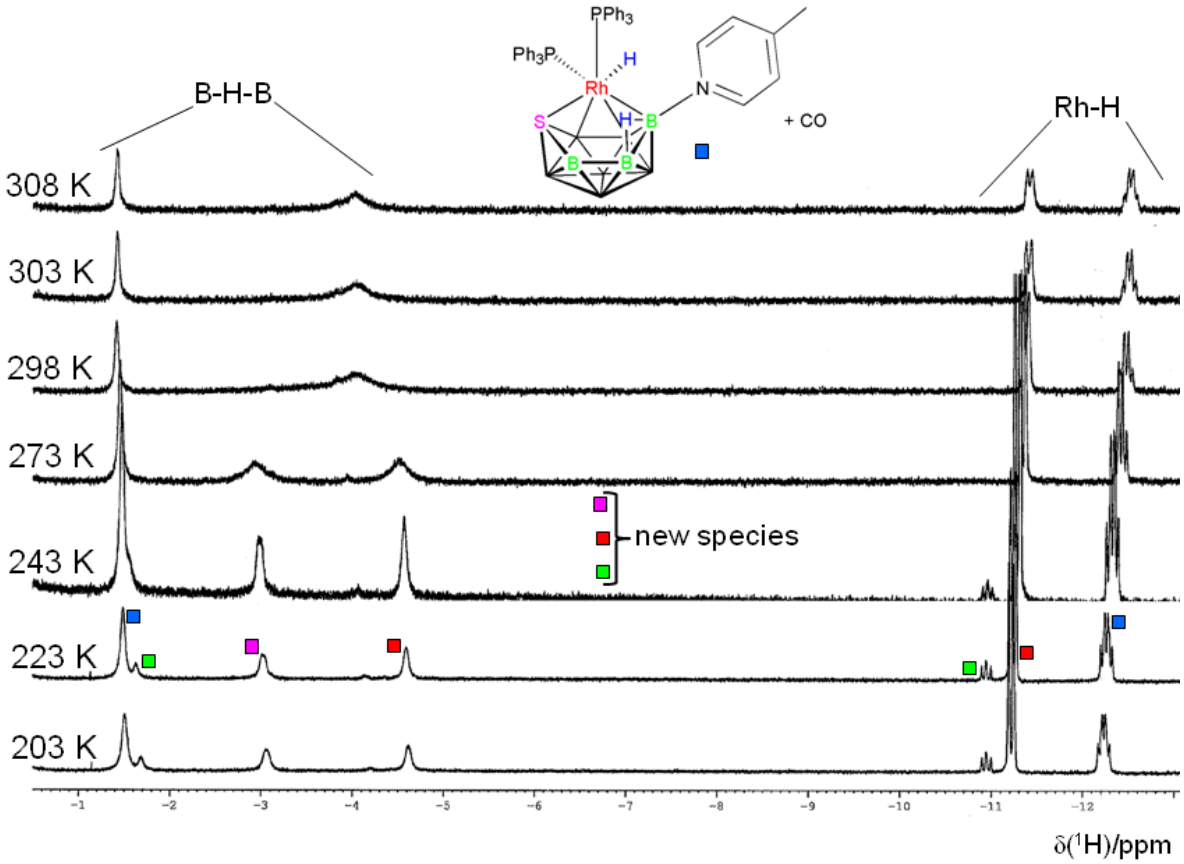

Figure 7 VT ^{1}H-{^{11}B} NMR spectra at different temperatures of **5** after treatment with CO. The peaks labelled with the blue squares correspond to the starting reactant, **5**.

For the 2-picoline system, a [^{31}P-^{1}H]-HMBC experiment at 223 K showed a correlation between the broad ^{31}P doublet of lower intensity and the hydride resonance (Figure S4). Similarly, the mixtures formed from the reactions of **2**, **4** and **5**, with CO, exhibited [^{31}P-^{1}H]-HMBC spectra with correlations between the highest intensity ^{31}P and ^{1}H doublets, and between the lowest intensity ^{31}P and ^{1}H signals (Figure 8).

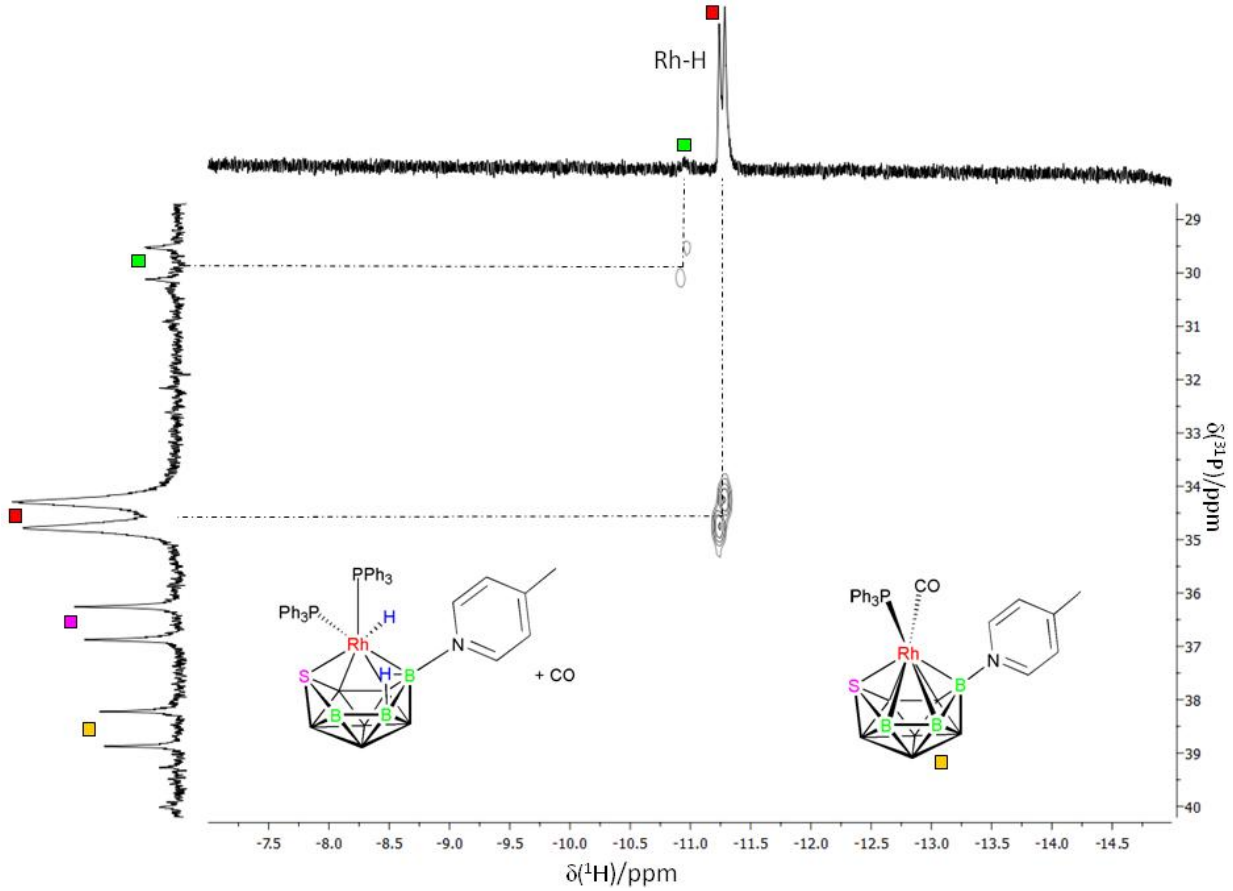

Figure 8 [^{31}P-^{1}H]-HMBC experiment at 223 K of **5** after treatment with CO.

Stereochemical non-rigidiy. The observations described above permit us to conclude that the reactions with CO lead to the formation of the substitution products, [8,8,8-(CO)(H)(PPh_3)-9-(L)-*nido*-8,7-$RhSB_9H_9$], where L = NC_5H_5, 2-Me-NC_5H_4, 3-Me-NC_5H_4 or 4-Me-NC_5H_4, which, according to the ^{1}H-{^{11}B} and ^{11}B-{^{1}H} NMR data (Figures S12 and S13), maintain the 11-vertex *nido*-cage of their *bis*-PPh_3-ligated precursors, **2**-**5**.

The data demonstrate the formation of two new species in the 2-picoline reaction system upon the treatment with CO, whereas, for the pyridine, 3- and 4-picoline-containing clusters, there are clearly three new compounds. These species are stable at low temperatures, but at room and higher temperatures they undergo hydrogen loss and a consequent *nido*-to-*closo* (or *isonido*) cluster structural transformation. The VT NMR data show that the intermediates interconvert. More specifically, it may be proposed that these labile rhodathiaboranes are isomers that exhibit different {Rh(CO)(H)(PPh_3)}-to-{η^4-SB_9H_9(L)} configurations (L = pyridine, 2-, 3- or 4-

picoline). In other words, the substitution of a PPh_3 ligand by a CO appears to enhance the stereochemical non-rigidity of the metal-thiaborane linkage, favouring isomerization processes.

The NMR data show that two of the three isomers detected in the reactions of CO with **2**, **4** and **5**, are very similar to the two species detected in the system with the 2-picoline counterpart, **3** (Figure S3 Figure 7). However, the interconversions between the species appear to be different.

A priory, these findings may be rationalized in terms of the different steric requirements of the 2-picoline substituent compared to pyridine, 3-picoline and 4-picoline resulting in different energy barriers for the transition states of the structural rearrangement processes together with stabilization of the products.

DFT study. In order to attain more insight into the fluxional and exchange processes involved in the compounds reported here, we carried out Density Functional Theory (DFT) calculations on model structures. The PPh_3 ligands were replaced by PH_3 to reduce calculational time.

Thus, DFT-calculations [8,8,8-(CO)(H)(PH_3)-9-(NC_5H_5)-*nido*-8,7-$RhSB_9H_9$] (**2a**) and [8,8,8-(CO)(H)(PH_3)-9-(2-Me-NC_5H_4)-*nido*-8,7-$RhSB_9H_9$] (**3a**) demonstrate that, of the six possible spatial combinations of the ligands around the metal centre, the most stable is that in which the hydride lies *trans* to the sulphur vertex, the CO ligand trans to the B(3)–B(4) edge and the PH_3 group occupies a position trans to the B(9) vertex (Figure 9). The pyridine and 2-picoline isomers, **2a_1-2a_6** and **3a_1-3a_6**, follow the same relative energy trend.

It is interesting to note that, for the 2-picoline-ligated isomers, the conformers in which the methyl group is adjacent to the pentagonal open face of the cluster are more stable than those in which this substituent is orientated towards the B(1) vertex. In some of the 2-picoline-ligated isomers, a conformational change around the N–B(9) bond has an energy penalty as large as 5.5 kcal/mol (see Figure S14).

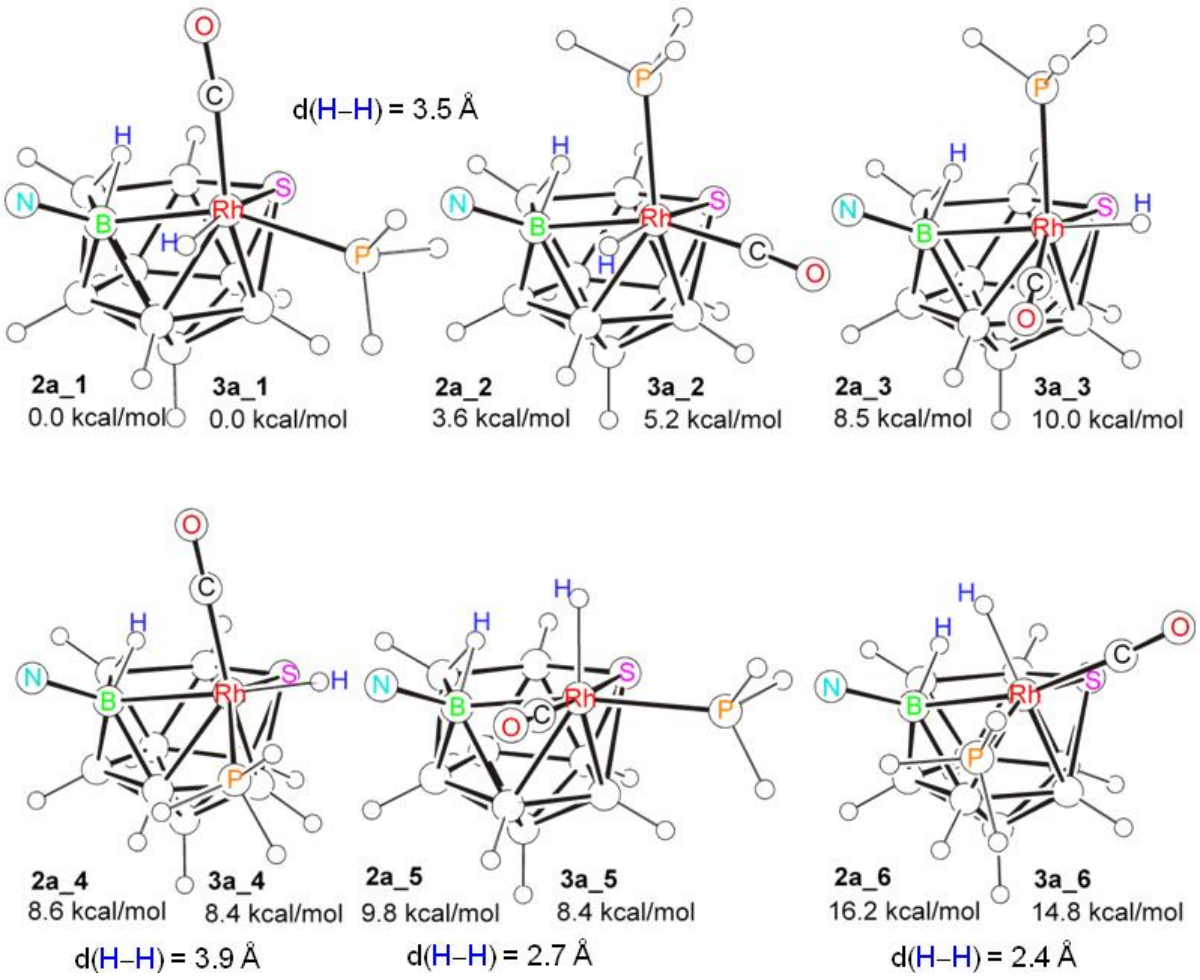

Figure 9 Energy comparisons for DFT optimized metal-to-thiaborane configurational isomers of the pyridine-ligated model, **2a** and of the 2-picoline-ligated counterpart, **3a**.

It has been previously demonstrated that substitution reactions of **2** with monodentate phosphines follow dissociative mechanisms, the dissociation of the PPh_3 ligand *trans* to the B(9) vertex being more favoured.[9] It is reasonable to expect, therefore, that the treatment of **2** and **3** with CO under the conditions described above (short reaction times and low temperatures) is more likely to result in the substitution of the PPh_3 *trans* to the B(9) vertex. Under this assumption, the PH_3-models, **2a_2** and **3a_2** would correspond to the kinetic reaction products; whereas the isomers, **2a_1** and **3a_1** would be the thermodynamic products (Figure 9).

Following this analysis, we can conclude that the major intermediate (red squares signals in Figures 5-8) is more likely to be the isomer with a metal-to-thiaborane configuration that

resembles that in **2a_2** and **3a_2** (Figure 9). A *pseudo*-rotation of the {Rh(H)(CO)(PPh_3)} group relative to the η^4-{SB_9H_9(L)} moiety can afford different metal-to-thiaborane configurations that can account for the intermediates that are observed by NMR at low temperatures.

A clockwise {Rh(H)(CO)(PH_3)}-to-η^4-{SB_9H_9(L)} rotation in the isomers, **2a_1, 2a_2, 3a_1** and **3a_2**, results in the formation of the corresponding isomers, **2a_6, 2a_5, 3a_6** and **3a_5**. These intermediates (Rh–H hydride *trans* to boron vertices) exhibit higher energies than the parent isomers [Rh–H hydride *trans* to S(7)]. However, this type of metal-thiaborane *pseudo*-rotation draws the B(9)–B(10) bridging hydrogen atom closer to the hydride ligand, facilitating its chemical exchange. Thus, intermediates **3a_5** and **3a_6** can account for the VT NMR behaviour observed in the 2-picoline system (Figures 5 and S3).

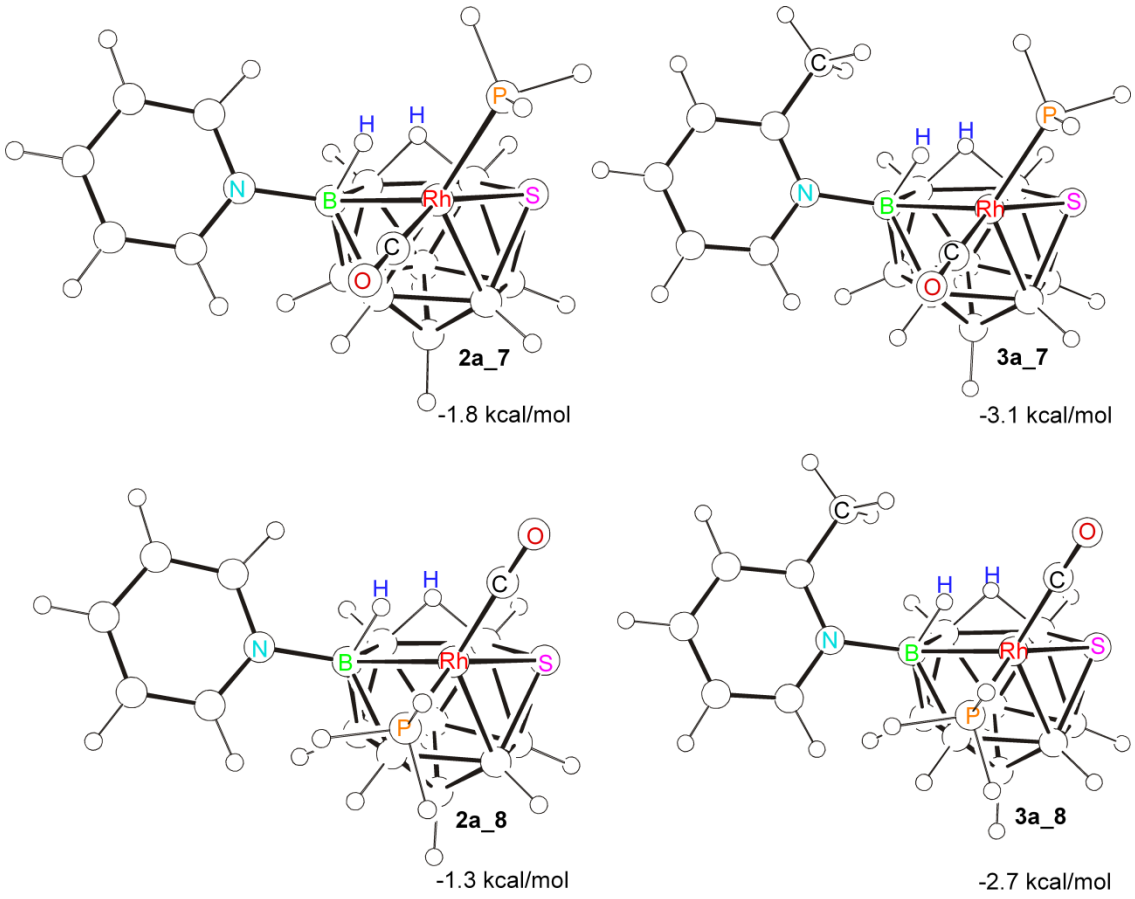

Figure 10 DFT-calculated rotational isomers for the PH_3-ligated models **2a** and **3a** with two hydrogen atoms on the pentagonal open face along the B(10)–B(11) and B(9)–Rh(8) edges.

Regarding the second major intermediate (purple squares in Figures 5-8), this species does not feature a Rh–H hydride ligand and therefore, the DFT-calculated isomers depicted in Figure 9 do not provide reasonable models that could account for the structure of this second derivative. Consequently, in the search for other plausible intermediates, we carried out DFT-calculations using as starting points isomers with bridging hydrogen atoms along the Rh(8)–B(9) and B(10)–B(11) edges of the pentagonal face. The optimizations gave isomers, **2a_7**, **2a_8**, **3a_7** and **3a_8**, of lower energy than the hydride-ligated clusters (Figures 9 and 10). On these calculated PH_3 models, one hydrogen atom occupies a position along the Rh(8)–B(9) edge in a clearly asymmetric fashion almost 2.0 Å from the metal centre, whereas the other hydrogen atom bridges the B(10)–B(11) edge (Figure 10). In this new configuration, these two hydrogen atoms are 2.06 Å apart, this allowing a facile chemical exchange between the two nuclear positions on the pentagonal open face. This fluxional process would lead to a single proton resonance in the negative region of the $^{1}H\text{-}\{^{11}B\}$ NMR spectra. Following this discussion, it is reasonable to propose that the second major isomer is a cluster that exhibits a nuclear configuration similar to that of the models, **2a_7**, **2a_8**, **3a_7** and **3a_8**, and that the two hydrogen atoms on the pentagonal face undergo fast exchange at both low and high temperatures, rendering both protons indistinguishable on the NMR time scale (purple squares in Figures 5-8). Related to this process is, for example, the low-energy barrier tautomerism of the *endo* / bridging H atoms in $[B_{11}H_{14}]^{-}$.[21]

In view of these DFT-results, it may be proposed that the hydride-ligated isomers found in the pyridine, 3- and 4-picoline systems, model **2a_2**, interconvert with the second major isomers, model **2a_7**, at higher temperatures (Scheme 6). Under the same conditions, the 2-picoline-ligated analogues do not undergo significant interconversion. However, as indicated above, the hydride-ligated species, represented by **3a_2**, undergo intramolecular exchange between the Rh–H hydride ligand and the B–H–B bridging hydrogen atom, most probably through metal-

thiaborane *pseudo*-rotations that bring the two hydrogen atoms closer, as suggested in the isomer **3a_5**.

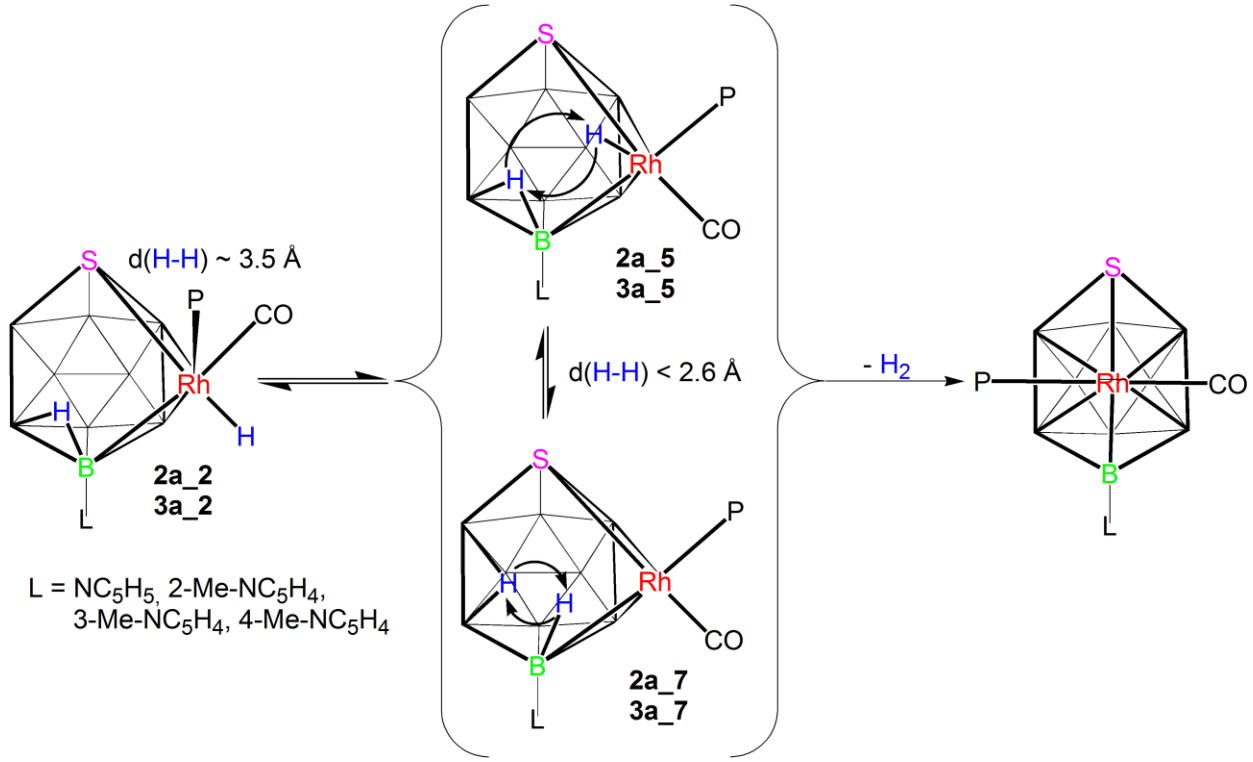

Scheme 6 Proposed tautomerization processes in CO-ligated rhodathiaboranes preceding H_2 loss.

The different behaviour in the interconversion of the CO-ligated pyridine, 3- and 4-picoline isomers *versus* the CO-ligated 2-picoline counterparts suggests that the rearrangement processes involved in the proposed **2a_2↔2a_5↔2a_7** tautomerizations, (Scheme 6) have lower energy barriers for the pyridine, 3-picoline and 4-picoline-ligated clusters than for the 2-picoline analogues. However, the exchange of the hydride ligand and the B–H–B bridging hydrogen atom, which should involve cluster rearrangements of the type, **2a_2↔2a_5** and **3a_2↔3a_5**, is favoured in the 2-picoline-ligated isomers, probably because the energy barrier between the hydride species, **3a_5**, and the other isomer, **3a_7**, is higher than in the pyridine, 3- and 4-picoline derivatives (Scheme 6).

It should be noted that a related mechanism of hydrogen M–H / B–H–M exchange, involving key M–(η^2-H_2) intermediates, has been reported for *exo-nido*-osmacarboranes that exhibit

{$Os(H)_2(PPh_3)_2$} fragments *exo*-polyhedrically linked to 11-vertex *nido*-carborane ligands, [7-R-7,9-$C_2B_9H_9$]$^{2-}$, via B–H two B–H–Os bonds.[22]

It is worth mentioning that the Rh(H)(CO)(L)}-to-η^4{SB_9H_9(L)} *pseudo*-rotations described earlier are related to the well known rotational twisting of *exo*-polyhedral metal-containing fragments bound through $(BH)_n$–M interactions to *nido*-carboranes.[23] In addition, the flexibility of heteroboranes as face-bound ligands is well documented in, for example, metallacarboranes and metallathiaboranes.[24] In the case of 11-vertex rhodathiaboranes, the parent cluster **1** undergoes an interesting fluxional process that involves a hindered rotation with respect the {SB_9H_{10}} fragment.[4] Recently, we have proved that the introduction of carbenes as *exo*-polyhedral ligands or protonation of the clusters results in an enhancement of the non-rigidity in the metal-to-thiaborane linkage, opening new ways of fluxional and exchange processes.[7-8,11] The CO ligand appears to induce an analogous lability in the meta-thiaborane connection.

Conclusions

It has been shown that the previously reported reaction between the rhodathiaborane [8,8-$(PPh_3)_2$-*nido*-8,7-$RhSB_9H_{10}$] (**1**) and pyridine to give the hydridorhodathiaborane, [8,8,8-(H)$(PPh_3)_2$-9-(NC_5H_5)-*nido*-8,7-$RhSB_9H_9$] (**2**), can extended to the 2-, 3- and 4-methylpyridine isomers, affording in good yields the corresponding picoline-ligated hydridorhodathiaboranes, **3-5**. These results illustrate the scope of this reaction that, in principle, can be carried out with a vast number of N-heterocyclic ligands.

The 3- and 4-picoline-ligated hydrides (**4** and **5**) exhibit a thermal stability toward dehydrogenation and *nido*-*closo* structural transformation that is similar to the pyridine counterpart, **2**. However, the 2-picoline analog loses hydrogen significantly faster.

The reactions of picoline-ligated hydridorhodathiaboranes (**3-5**) with C_2H_4 and CO in this report resemble those found for the pyridine analog, **2**, giving products of ligand substitution and cluster dehydrogenation (**12-19**). These reactions nicely illustrate the structural flexibility and chemical tunability of these 11-vertex clusters and demonstre that the parent rhodathiaborane,

[8,8-$(PPh_3)_2$-*nido*-8,7-$RhSB_9H_{10}$] (**1**), first reported in 1990,[4] is actually a rich source of organometallic chemistry.

The study of the reactions between the hydridorhodathiaboranes and CO at low temperatures has allowed the identification of intermediates that have provided new insights into the loss of hydrogen from the clusters. Upon the substitution of one of the PPh_3 ligands by CO, the clusters become more reactive, undergoing, at low temperature, intramolecular as well as intermolecular exchange processes that are a consequence of the increased cluster non-rigidity. The dynamic behavior observed for the 2-picoline system is different to that of the pyridine, 3- and 4-picoline systems, with DFT calculations supporting the proposition that the difference in cluster fluxionality may be attributed to the steric effect of the methyl group of the 2-methyl-pyridine substituent. The intramolecular exchange between the hydride ligand and the B–H–B bridging hydrogen atom found at low temperatures for the 2-picoline system is also relevant here because it should involve a transition state in which the two hydrogen atoms reach a close proximity in the cluster, representing therefore, a crucial step towards hydrogen loss. Although the detailed mechanism is unclear, the formation of Rh–(η^2-H_2) intermediates could facilitate the exchange of the hydrogen atoms at low temperatures. In this regard, we have recently reported that dihydrogen activation on a carbene-ligated rhodathiaborane takes place through structural transformations of the cluster, involving the formation of dihydrogen-ligated intermediates.[7] For the carbonyl intermediates, the final release could occur similarly via H_2 coordination to the rhodium centre.

Table 1. Selected interatomic distances (Å) and angles (◦) between interatomic vectors with standard uncertainties (s.u) in parentheses for [8,8,8-(H)(PPh_3)$_2$-9-(NC_5H_4)-*nido*-8,7-$RhSB_9H_9$] (**2**), [8,8,8-(H)(PPh_3)$_2$-9-(3-Me-NC_5H_4)-*nido*-8,7-$RhSB_9H_9$] (**4**), [8,8,8-(H)(PPh_3)$_2$-9-(4-Me-NC_5H_4)-*nido*-8,7-$RhSB_9H_9$] (**5**) and [8,8,8-(H)($PMePh_2$)$_2$-9-(NC_5H_4)-*nido*-8,7-$RhSB_9H_9$] (**6**).

	2[6a]	**4**	**5**	**6**[9]
Rh(8)-S(7)	2.431(2)	2.4132(8)	2.4373(14)	2.4270(5)
Rh(8)-P(1)	2.354(2)	2.3752(8)	2.3488(14)	2.3224(6)
Rh(8)-P(2)	2.341(2)	2.3383(7)	2.3560(14)	2.3091(6)
Rh(8)-B(3)	2.201(10)	2.235(3)	2.239(6)	2.230(2)
Rh(8)-B(4)	2.217(11)	2.236(3)	2.216(5)	2.209(2)
Rh(8)-B(9)	2.220(9)	2.208(3)	2.210(6)	2.214(2)
S(7)-B(2)	1.980(9)	1.991(3)	1.984(6)	1.996(3)
S(7)-B(3)	2.059(11)	2.085(3)	2.041(6)	2.060(3)
S(7)-B(11)	1.953(9)	1.909(3)	1.943(6)	1.928(3)
N(1)-B(9)	1.547(11)	1.569(3)	1.555(7)	1.556(3)
B(6)-B(11) (shortest)	1.727(14)	1.738(4)	1.741(8)	1.748(4)
B(2)-B(3) (longest)	1.906(14)	1.902(4)	1.915(9)	1.913(4)
B(9)-B(10)	1.856(14)	1.868(4)	1.870(8)	1.874(3)
P(1)-Rh(8)-P(2)	100.27(7)	101.68(3)	101.77(5)	98.10(2)
S(7)-Rh(8)-P(1)	96.38(7)	103.16(3)	96.81(5)	97.82(2)
S(7)-Rh(8)-P(2)	102.05(8)	97.63(3)	101.03(5)	105.080(19)
Rh(8)-B(9)-N(1)	120.6(5)	120.81(16)	121.6(4)	119.30(15)
S(7)-Rh(8)-B(9)	87.1(3)	88.17(7)	88.02(15)	87.79(6)
P(1)-Rh(8)-B(9)	162.4(3)	157.80(8)	159.02(15)	163.22(6)
P(2)-Rh(8)-B(9)	95.8(3)	95.54(8)	97.28(15)	95.66(6)

Table 2 ^{11}B and ^{1}H NMR data for [8,8,8-(H)(PPh$_3$)$_2$-9-(2-Me-NC$_5$H$_4$)-*nido*-8,7-RhSB$_9$H$_9$] (**3**) [8,8,8-(H)(PPh$_3$)$_2$-9-(3-Me-NC$_5$H$_4$)-*nido*-8,7-RhSB$_9$H$_9$] (**4**) and [8,8,8-(H)(PPh$_3$)$_2$-9-(4-Me-NC$_5$H$_4$)-*nido*-8,7-RhSB$_9$H$_9$] (**5**) in CD_2Cl_2 compared to the corresponding DFT/GIAO-calculated ^{11}B-nuclear shielding values calculated for the PH$_3$-models [in brackets]

	3			**4**			**5**		
Assignments[a]	$\delta(^{11}B)$		$\delta(^{1}H)$[b]	$\delta(^{11}B)$		$\delta(^{1}H)$[b]	$\delta(^{11}B)$		$\delta(^{1}H)$[b]
9[c]	+11.1	[+18.8]	2-Me-NC$_5$H$_4$	+12.1	[+17.9]	3-Me-NC$_5$H$_4$	+11.8	[+17.6]	4-Me-NC$_5$H$_4$
3	+6.1[d]	[+8.5]	+3.42	+8.1	[+8.9]	+3.51	+7.8[e]	[+9.4]	+3.53
6	+4.0	[+5.5]	+3.03	+3.9	[+7.5]	+2.60	+3.3	[+7.4]	+2.63
11	+1.5	[+2.1]	+3.58	+0.6	[+2.2]	+4.13	+0.2[f]	[+2.2]	+4.13
4	-3.9	[+1.9]	+3.26	-3.7	[-0.1]	+2.85	-3.8	[-0.1]	+2.85
5	-12.1[g]	[-14.0]	+1.93	-10.0[h]	[-11.1]	+1.83	-10.2[i]	[-10.7]	+1.81
10	-14.4	[-19.2]	+1.06	-17.9	[-22.7]	+0.92	-17.9	[-23.0]	+0.88
1	-25.0[j]	[-23.8]	+1.49	-25.6	[-25.4]	+1.50	-25.7	[-25.1]	+1.49
2	-27.2	[-27.9]	+1.21	-29.1	[-28.5]	+1.11	-28.5	[-28.4]	+1.09
μ(9, 10)			-0.95			-1.38			-1.42
Rh(8)-H			-12.49[k]			-12.47[l]			-12.43[m]

[a]Assignments based on ^{1}H–{^{11}B} selective experiments and DFT calculations.[b] Proton chemical shifts corresponding to boron-bound hydrogen atoms.[c] Picoline-substituted vertex.[d] $^{1}J(^{11}B–^{1}H)$ = 132 Hz.[d] $^{1}J(^{11}B–^{1}H)$ = 112 Hz.[e] $^{1}J(^{11}B–^{1}H)$ = 127 Hz. [f] $^{1}J(^{11}B–^{1}H)$ = 142 Hz.[g] $^{1}J(^{11}B–^{1}H)$ = 140 Hz.[h] $^{1}J(^{11}B–^{1}H)$ = 137 Hz.[i] $^{1}J(^{11}B–^{1}H)$ = 146 Hz.[j] $^{1}J(^{11}B–^{1}H)$ = 150 Hz.[k] Apparent quartet: $^{1}J(^{103}Rh–^{1}H) + ^{2}J(^{31}P_A–^{1}H) + ^{2}J(^{31}P_B–^{1}H) \approx 17$ Hz.[l] Apparent quartet: $^{1}J(^{103}Rh–^{1}H) + ^{2}J(^{31}P_A–^{1}H) + ^{2}J(^{31}P_B–^{1}H) \approx 17$ Hz.[m] Apparent quartet: $^{1}J(^{103}Rh–^{1}H) + ^{2}J(^{31}P_A–^{1}H) + ^{2}J(^{31}P_B–^{1}H) \approx 20$ Hz; ^{1}H-{^{31}P}: -12.43 [d, $^{1}J(^{103}Rh–^{1}H)$ = 19.7 Hz, H].

Table 3 ^{11}B and ^{1}H NMR data for [1,1-$(PPh_3)_2$-3-(NC_5H_5)-*isonido*-1,2-$RhSB_9H_9$] (**8**), [1,1-$(PPh_3)_2$-3-(2-Me-NC_5H_4)-*closo*-1,2-$RhSB_9H_8$] (**9**), [1,1-$(PPh_3)_2$-3-(3-Me-NC_5H_4)-*closo*-1,2-$RhSB_9H_8$] (**10**) and [1,1-$(PPh_3)_2$-3-(4-Me-NC_5H_4)-*closo*-1,2-$RhSB_9H_8$] (**11**) in CD_2Cl_2 compared to the corresponding DFT/GIAO-calculated ^{11}B-nuclear shielding values [in brackets].

	8[6b]		**9**		**10**		**11**	
Assig.[a]	$\delta(^{11}B)$	$\delta(^{1}H)$[b]	$\delta(^{11}B)$	$\delta(^{1}H)$[b]	$\delta(^{11}B)$	$\delta(^{1}H)$[b]	$\delta(^{11}B)$	$\delta(^{1}H)$[b]
3[c]	+54.6 [+58.4]	NC_5H_5	+53.3 [+57.8]	2-Me-NC_5H_4	+54.8 [+59.0]	3-Me-NC_5H_4	+54.9 [+59.5]	4-Me-NC_5H_4
9	+27.3[d] [+30.1]	+4.09	+25.4 [+29.7]	+4.32	+27.5 [+30.2]	+4.24	+27.3[e] [+29.6]	+4.09
4, 5	-0.5 [+6.7,+5.4]	+1.27	-0.6 [+10.8, +3.1]	+1.27	+0.5 [+7.9, +4.1]	+1.28	-0.7 [+8.4, +3.4]	+1.29 (2H)
8	-15.2 [-12.2]	+2.16	-14.2 [-13.1]	+2.40	-14.3 [-12.6]	+2.37	-15.5 [-12.9]	+2.17
6, 7	-24.2[f] [-18.1, -21.8]	-0.22 (2H)	-21.9 [-15.4, -23.0]	+0.05 (4H)	-23.8 [-14.8, -22.4]	-0.10 (2H)	-24.6 [-14.1, -22.0]	-0.23 (4H)
10,11	-34.4[g] [-29.3, -29.6]	-0.27 (2H)	-29.8 [-26.5, -31.1]		-29.9 [-28.8, -29.5]	-0.29 (2H)	-30.7 [-28.0, -29.7]	

[a]Assignments based on ^{1}H–{^{11}B} selective experiments and DFT calculations.[b] Proton chemical shifts corresponding to boron-bound hydrogen atoms.[c] Picoline-substituted vertex.[d] $^{1}J(^{11}B–^{1}H)$ = 144 Hz.[e] $^{1}J(^{11}B–^{1}H)$ = 137 Hz.[f] $^{1}J(^{11}B–^{1}H)$ = 129 Hz.[g] $^{1}J(^{11}B–^{1}H)$ = 139 Hz.

Table 4 ^{11}B and ^{1}H NMR data for [1,1-(PPh$_3$)(η^2-C$_2$H$_4$)-3-(NC$_5$H$_5$)-*isonido*-1,2-RhSB$_9$H$_8$] (**12**), [1,1-(PPh$_3$)(η^2-C$_2$H$_4$)-3-(2-Me-NC$_5$H$_4$)-*closo*-1,2-RhSB$_9$H$_8$] (**13**), [1,1-(PPh$_3$)(η^2-C$_2$H$_4$)-3-(3-Me-NC$_5$H$_4$)-*closo*-1,2-RhSB$_9$H$_8$] (**14**) and [1,1-(PPh$_3$)(η^2-C$_2$H$_4$)-3-(4-Me-NC$_5$H$_4$)-*closo*-1,2-RhSB$_9$H$_8$] (**15**) in CD_2Cl_2 compared to the corresponding DFT/GIAO-calculated ^{11}B-nuclear shielding values [in brackets].

	12[ba]			**13**		**14**		**15**	
Assig.[a]	δ(^{11}B)		δ(^{1}H)[b]	δ(^{11}B)	δ(^{1}H)[b]	δ(^{11}B)	δ(^{1}H)[b]	δ(^{11}B)	δ(^{1}H)[b]
3[c]	+55.7	[+58.5]	NC$_5$H$_5$	+54.9	2-Me-NC$_5$H$_4$	+56.3	3-Me-NC$_5$H$_4$	+55.3	4-Me-NC$_5$H$_4$
9	+26.4[a]	[+28.5]	+4.36	+24.9[e]	+4.27	+26.2[f]	+4.22	+26.2[g]	+4.33
5	+0.8	[+9.0]	+1.80	+4.0	+2.01	+1.4	+1.93	+0.1	+2.05
4	-0.1	[+4.2]	+2.06	-1.1	+1.58	-0.1	+1.65	-0.7	+1.72
8	-14.5	[-13.3]	+2.46	-14.1	+2.53	-14.6	+2.30	-15.3	+2.45
7	-22.2	[-16.8]	+0.54	-20.4	+0.87	-22.6	+0.37	-22.5	+0.39
6	-24.6	[-22.0]	-0.17	-25.4[h]	-0.54	-24.6	-0.23	-25.1	-0.23
10,11	-30.3	[-27.4] [-27.0]	+0.42, -0.01	-29.1 -29.8	+0.23 -0.10	-30.0 -30.7	+0.19 -0.21	-30.0	+0.53, -0.01

[a]Assignments based on ^{1}H–{^{11}B} selective experiments and DFT calculations.[b] Proton chemical shifts corresponding to boron-bound hydrogen atoms.[c] Picoline-substituted vertex.[d] ^{1}J(^{11}B–^{1}H) = 124 Hz.[e] ^{1}J(^{11}B–^{1}H) = 127 Hz.[f] ^{1}J(^{11}B–^{1}H) = 124 Hz.[g] ^{1}J(^{11}B–^{1}H) = 127 Hz.[h] ^{1}J(^{11}B–^{1}H) = 134 Hz.

Table 5 ^{11}B and ^{1}H NMR data for [1,1-(PPh_3)(CO)-9-(NC_5H_5)-*closo*-1,2-$RhSB_9H_9$] (**16**), [1,1-(PPh_3)(CO)-3-(2-Me-NC_5H_4)-*closo*-1,2-$RhSB_9H_8$] (**17**), [1,1-(PPh_3)(CO)-3-(3-Me-NC_5H_4)-*closo*-1,2-$RhSB_9H_8$] (**18**) and [1,1-(PPh_3)(CO)-3-(4-Me-NC_5H_4)-*closo*-1,2-$RhSB_9H_8$] (**19**) in CD_2Cl_2 compared to the corresponding DFT/GIAO-calculated ^{11}B-nuclear shielding values [in brackets].

	16[6b]			**17**			**18**			**19**		
Assig.[a]	$\delta(^{11}B)$		$\delta(^{1}H)$[b]	$\delta(^{11}B)$		$\delta(^{1}H)$[b]	$\delta(^{11}B)$		$\delta(^{1}H)$[b]	$\delta(^{11}B)$		$\delta(^{1}H)$[b]
3[c]	+55.4	[+59.5]	NC_5H_5	+53.8	[+57.7]	2-Me-NC_5H_5	+55.7	[+59.7]	3-Me-NC_5H_5	+55.3	[+58.7]	4-Me-NC_5H_5
9	+28.1[d]	[+30.4]	+4.34	+27.4[e]	[+29.2]	+4.34	+28.2[f]	[+30.1]	+4.33	+28.2	[+29.7]	+4.44
5	+1.1	[+8.9]	+2.39	+0.97 (2B)	[+14.2]	+2.40	+1.2	[+8.8]	+2.40	+1.5	[+12.2]	+2.50
4	-0.7	[+4.2]	+1.08		[+0.8]	+1.33	-0.7	[+4.2]	+1.12	-0.5	[+1.3]	+1.21
8	-14.4	[-13.4]	+2.37	-13.6	[-14.3]	+2.40	-14.7	[-13.6]	+2.40	-14.4	[-14.4]	+2.50
6	-24.4	[-17.1]	+0.66	-22.9	[-17.2]	+0.73	-24.9	[-17.1]	+0.65	-24.5	[-17.3]	+0.68
7	-26.1	[-21.8]	-0.08	-24.9	[-22.9]		-26.1	[-21.6]	+0.03	-25.9	[-24.1]	+0.22
10, 11	-31.9[g]	[-26.7] [-29.2]	+0.07 0.00	-31.8[h]	[-24.0] [-30.6]	+0.01 (3H)	-32.0	[-26.8] [-29.3]	-0.01 (2H)	-31.9[i]	[-25.9] [-29.7]	+0.15 (2H)

[a]Assignments based on $^{1}H\{^{11}B\}$ selective experiments and DFT calculations.[b] Proton chemical shifts corresponding to boron-bound hydrogen atoms.[c] Picoline-substituted vertex.[d] $^{1}J(^{11}B\text{-}^{1}H)$ = 118 Hz.[e] $^{1}J(^{11}B\text{-}^{1}H)$ = 129 Hz.[f] $^{1}J(^{11}B\text{-}^{1}H)$ = 133 Hz.[g] $^{1}J(^{11}B\text{-}^{1}H)$ = 127 Hz.[h] $^{1}J(^{11}B\text{-}^{1}H)$ = 138 Hz.[i] $^{1}J(^{11}B\text{-}^{1}H)$ = 142 Hz.[j] $^{1}J(^{11}B\text{-}^{1}H)$ = 138 Hz.

Table 7 Selected interatomic distances (Å) and angles (◦) between interatomic vectors with standard uncertainties (s.u) in parentheses for [1,1-$(PPh_3)_2$-3-(NC_5H_5)-*isonido*-8,7-$RhSB_9H_9$] (**8**), [1,1-$(PPh_3)_2$-3-(2-Me-NC_5H_4)-*closo*-8,7-$RhSB_9H_8$] (**9**), [1,1-$(PPh_3)(PMe_3)$-3-(NC_5H_5)-*closo*-8,7-$RhSB_9H_8$] (**20**) and [1,1-$(PMe_2Ph)_2$-3-(NC_5H_5)-*closo*-8,7-$RhSB_9H_8$] (**21**).

	8[10]	**9**	**20**	**21**
Rh(1)-S(2)	2.3997(14)	2.3885(14)	2.3841(9)	2.3826(11)
Rh(1)-P(1)	2.3278(13)	2.3276(15)	2.2889(10) [PMe_3]	2.2821(11)
Rh(1)-P(2)	2.3012(12)	2.3243(15)	2.2710(9) [PPh_3]	2.2741(11)
Rh(1)-B(3)	2.085(6)	2.119(7)	2.087(4)	2.067(4)
Rh(1)-B4)	2.400(6)	2.435(7)	2.401(4)	2.362(5)
Rh(1)-B(5)	2.562(6)	2.485(7)	2.471(4)	2.487(5)
Rh(1)-B(6)	2.344(6)	2.364(7)	2.380(4)	2.333(4)
Rh(1)-B(7)	2.387(6)	2.372(7)	2.354(4)	2.409(5)
S(2)-B(4)	1.918(6)	1.934(8)	1.953(4)	1.932(5)
S(2)-B(5)	1.956(6)	1.921(7)	1.937(4)	1.969(5)
S(2)-B(8)	1.989(6)	2.001(7)	1.999(5)	1.989(5)
N-B(3)	1.532(8)	1.556(7)	1.546(5)	1.541(5)
B(3)-B(7) (shortest)	1.709(8)	1.716(10)	1.705(5)	1.712(6)
B(4)-B(8) (longest)	1.893(9)	1.905(10)	1.917(6)	1.916(7)
P(1)-Rh(1)-P(2)	96.97(4)	97.86(5	96.68(4)	96.27(4)
P(1)-Rh(1)-S(2)	102.32(5)	107.75(5)	103.17(4)	103.77(4)
P(2)-Rh(1)-S(2)	110.83(5)	103.80(5)	110.92(3)	112.02(4)
P(1)-Rh(1)-B(3)	112.65(17)	112.83(19)	114.79(11)	116.40(12)
P(2)-Rh(1)-B(3)	112.42(16)	112.3(2)	108.42(11)	104.50(13)
B(3)-Rh(1)-S(2)	119.02(16)	119.79(18)	120.32(11)	121.22(12)

Experimental Section

General Considerations: All reactions were carried out under an argon atmosphere using standard Schlenk-line techniques. Solvents were obtained from an Innovative Technology Solvent Purification System. All commercial reagents were used as received without further purification. The rhodathiaboranes [8,8-$(PPh_3)_2$-*nido*-8,7-$RhSB_9H_{10}$] (**1**) was prepared by published methods.[4]

^{1}H and ^{11}B NMR data, focused on cluster B–H units, are gathered in Tables 3-5. Additional ^{1}H NMR data are below.

NMR spectra were recorded on Bruker Avance 300-MHz, AV 400-MHz and AV 500 MHz spectrometers, using ^{11}B, ^{11}B–{^{1}H}, ^{1}H, ^{1}H–{^{11}B}, ^{1}H–{^{11}B(selective)},[25] ^{31}P–{^{1}H}, [^{1}H–^{1}H]–NOESY and [^{1}H–^{31}P]–HMBC techniques.[26] ^{1}H chemical shifts were measured relative to partially deuterated solvent peaks but are reported in ppm relative to tetramethylsilane. ^{11}B chemical shifts were measured relative to [$BF_3(OEt)_2$)]. ^{31}P chemical shifts were measured relative to H_3PO_4 (85%). Mass spectrometry data were recorded on a VG Autospec double focusing mass spectrometer, on a microflex MALDI–TOF, and on a ESQUIRE 3000+ API–TRAP, operating in either positive or negative modes. In each case there was an excellent correspondence between the calculated and measured isotopomer envelopes. A well-matched isotope pattern may be taken as a good criterion of identity.[27]

GC analyses were performed either on a Hewlett-Packard HP 5890 Series II gas chromatograph equipped with a flame ionization detector and a 25 m (0.32 mm inner diameter, 0.17 mm film thickness) HP-Ultra-1 column, or on an Agilent 6890 Series GC System equipped with an Agilent 5973 mass-selective detector and a 30 m (0.25 mm i.d.,0.25 mm f.t.) HP-5MS column.

X-ray structure analysis of crystals 4, 5 and 9: Crystals were grown by slow diffusion of hexane into dichloromethane solutions. In all cases, the crystals were coated with perfluoropolyether, mounted on a glass fiber and fixed in a cold nitrogen stream (T = 100(2) K) to the goinometer head. Data collection were performed on a Bruker Kappa APEX DUO CCD area detector diffractometer with monochromatic radiation $\lambda(Mo_{K\alpha})$ = 0.7107073 Å, using narrow frames (0.3° in ω). The data were reduced (SAINT)[28] and corrected for absorption effects by multiscan methods (SADABS).[29] The structure was solved using the SHELXS-86 program,[30] and refined against all F^2 data by full-matrix least-squares techniques (SHELXL-97).[31] All non-hydrogen atoms were refined with anisotropic displacement parameters. Hydrogen atoms were included in calculated positions and refined with a positional and thermal riding model.

Calculations

All DFT calculations were performed using the Gaussian 09 package.[32] Structures were initially optimized using standard methods with the STO-3G* basis-sets for C, B, P, S, and H with the LANL2DZ basis-set for the rhodium atom. The final optimizations, including frequency analyses to confirm the true minima, were performed using B3LYP methodology, with the 6-31G* and LANL2DZ basis-sets. The GIAO nuclear shielding calculations were performed on the final optimized geometries, and computed ^{11}B shielding values were related to chemical shifts by comparison with the computed value for B_2H_6, which was taken to be $\delta(^{11}B)$ +16.6 ppm relative to the $BF_3(OEt_2)$ = 0.0 ppm standard.

Synthesis of picoline-ligated 11-vertex hydridorohodathiaboranes (3–5)

[8,8,8-H(PPh$_3$)$_2$-9-(2-Me-NC$_5$H$_4$)-*nido*-8,7-RhSB$_9$H$_9$] (3). In a Schlenk tube, 100 mg (0.130 mmol) of **1** was dissolved in 10 mL of CH_2Cl_2, resulting in a bright-red solution. 190 µl (182mg, 1.95 mmol) of 2-methylpyridine was syringed into the solution, and the reaction mixture was stirred at room temperature for 4 hours to give a 1:1 mixture of **3**, and its dehydrogenation product, [1,1-(PPh$_3$)$_2$-3-(2-Me-Py)-*closo*-1,2-RhSB$_9$H$_8$]. This mixture was cooled to the liquid nitrogen temperature, the vessel evacuated, and then exposed to a hydrogen filled balloon. The resulting system was stirred at room temperature for 4 hours. After this time, the solvent was evaporated to dryness and the residue washed three times with CH_2Cl_2/hexane, to obtain **3**. Yield: 97.0 mg, 0.112 mmol, 87%. Anal. Calcd for $C_{42}H_{47}B_9N_1P_2Rh_1S_1$: C, 58.65; H, 5.51; N, 1.63; S, 3.73. Found: C, 58.23; H, 5.41; N, 1.25; S, 3.98. IR (ATR): *v* 2502 vs (BH), 2042 m (RhH). ^{1}H NMR (300 MHz, CD_2Cl_2, 300 K): δ 8.97 (d, 2H, 2-CH$_3$-NC$_5$*H$_4$*), 8.02 (m, 1H, 2-CH$_3$-NC$_5$*H$_4$*), 7.69 (m, 1H, 2-CH$_3$-Py), 7.23-7.00 (30H, 2PPh$_3$), 3.10 (s, 3H, 2-C*H*$_3$- Py). ^{31}P-{^{1}H} NMR (121 MHz, CD_2Cl_2, 300 K): δ +34.5 [br dd, $^1J_{RhP}$ = 97.66 Hz, $^2J_{PP}$ no resolved due to the broadness of the peak], +32.6 [dd, $^1J_{RhP}$ = 129 Hz, $^2J_{PP}$ = 18.3 Hz]. ^{31}P-{^{1}H} NMR (121 MHz, CD_2Cl_2, 243 K): δ +36.6 [br dd, $^1J_{RhP}$ = 106 Hz, $^2J_{PP}$ no resolved due to the broadness of the peak], +32.3 [dd, $^1J_{RhP}$ = 125 Hz, $^2J_{PP}$ = 19 Hz] LRMS (MALDI$^+$): *m/z* 596 [M - (PPh$_3$) - 2H]$^+$. Isotope envelopes match those calculated from the known isotopic abundances of the constituent elements.

[8,8,8-H(PPh$_3$)$_2$-9-(3-Me-NC$_5$H$_4$)-*nido*-8,7-RhSB$_9$H$_9$] (4). To a bright-yellow solution of 100 mg (0.131 mmol) of **1** in 10 mL de CH_2Cl_2, 127 µl (121 mg; 1.30 mmol) of 3-methylpyridine was added. After 4 hours of stirring at room temperature under an atmosphere of argon, the solvent was evaporated to dryness and the solid residue washed three times with hexane. The final product was characterized as compound **4**. Yield: 91.0 mg, 0.106 mmol, 81%. Anal. Calcd for $C_{42}H_{47}B_9N_1P_2Rh_1S_1 \cdot 2CH_2Cl_2$: C, 51.31; H, 4.99; N, 1.36; S, 3.11. Found: C, 50.82; H, 5.03; N, 1.31; S, 2.35. IR (ATR): *v* 2529 vs (BH), 2040 m (RhH). ^{1}H NMR (300 MHz, CD_2Cl_2, 300 K): δ 7.96 (m, 2H; 3-CH$_3$-NC$_5$*H*$_4$), 7.68 (m, 1H; 3-CH$_3$-NC$_5$*H*$_4$), 7.33 (t, 1H; 3-CH$_3$-NC$_5$*H*$_4$), 7.31-7.04 (30H, 2PPh$_3$), 2.20 (s, 3H, 3-C*H*$_3$-NC$_5$H$_4$). ^{31}P–{^{1}H} NMR (121 MHz, CD_2Cl_2, 300 K): +32.7 [d, $^1J_{RhP}$ = 120 Hz; 2PPh$_3$]. ^{31}P–{^{1}H} NMR (121 MHz, CD_2Cl_2, 243 K) δ +35.7 [br dd, $^1J_{RhP}$ = 103 Hz; $^2J_{PP}$ not resolved due to the broadness of the peak], +30.7 [dd, $^1J_{RhP}$ = 128 Hz; $^2J_{PP}$ = 19 Hz]. LRMS (MALDI$^+$): *m/z* 596 [M - (PPh$_3$) - 2H]$^+$. Isotope envelopes match those calculated from the known isotopic abundances of the constituent elements.

[8,8,8-H(PPh$_3$)$_2$-9-(4-Me-NC$_5$H$_4$)-*nido*-8,7-RhSB$_9$H$_9$] (5). In a Schlenk tube, a solution of **1** (300 mg, 0.393 mmol) in 15 mL of CH_2Cl_2 was treated with 381 µl (363 mg; 3.90 mmol) of 4-methylpyridine. The reaction mixture was stirred at room temperature under an atmosphere of argon for 4 hours, the solvent was evaporated to dryness and the residue was washed three times with hexane to isolate **5**. Yield: 255 mg, 0.296 mmol, 75%. Anal. Calcd for $C_{42}H_{47}B_9N_1P_2Rh_1S_1 \cdot CH_2Cl_2$: C, 54.65; H, 5.23; N, 1.48; S, 3.39. Found: C, 54.18; H, 5.48; N, 1.46; S, 3.41. IR (ATR): *v* 2520 vs (BH), 2465 vs (BH), 2033 m (RhH). ^{1}H NMR (300 MHz, CD_2Cl_2, 300 K): δ 7.70 (d, 2H; 4-CH$_3$-NC$_5$*H*$_4$), 7.36 (t, 2H; 4-CH$_3$-NC$_5$*H*$_4$), 7.26-6.85(30H, 2PPh$_3$), 2.27 (m, 3H, 4-C*H*$_3$-NC$_5$H$_4$). ^{31}P{^{1}H} NMR (121 MHz, CD_2Cl_2, 300 K): δ 33.0 [d, ^1J (Rh, P) = 121 Hz; 2PPh$_3$]. ^{31}P-{^{1}H} NMR (121 MHz, CD_2Cl_2, 203 K) δ 37.0 [br dd, $^1J_{RhP}$ = 107 Hz; $^2J_{PP}$ no resolved due to the broadness of the peak], 30.0 [dd, $^1J_{RhP}$ = 128 Hz; $^2J_{PP}$ = 18 Hz]. LRMS (MALDI$^+$): *m/z* 596 [M - (PPh$_3$) - 2H]$^+$. Isotope envelopes match those calculated from the known isotopic abundances of the constituent elements.

Preparation of *bis*-PPh_3-ligated *closo*-rhodathioboranos (9-11). As a general procedure, a 10-fold excess of PPh_3 was added to a solution of the corresponding ethylene-ligated rhodathiaboranes, **13**-**15**, which were dissolved in 10 mL of CH_2Cl_2. The orange-red solution was stirred at room temperature for several hours to give a red solution. The solvent was evaporated to dryness and the residue washed three times with hexane. The final solids were recrystallized from CH_2Cl_2/hexane to give the *bis*-PPh_3-ligated rhodathiaboranes, [1,1-$(PPh_3)_2$-3-(L)-*closo*-1,2-$RhSB_9H_8$], where L= 2-Me-NC_5H_4 (**9**), 3-Me-NC_5H_4 (**10**) or 4-Me-NC_5H_4 (**11**).

[1,1-$(PPh_3)_2$-3-(2-Me-NC_5H_4)-*closo*-1,2-$RhSB_9H_8$] (9). The reaction was carried out with 120 mg (0.458 mmol) of PPh_3 and 30 mg (0.048 mmol) of [1,1-$(PPh_3)(\eta^2$-$C_2H_4)$-3-(2-Me-NC_5H_4)-*closo*-1,2-$RhSB_9H_8$] (**13**), stirring for 6 h. Yield: 35 mg, 0.0408 mmol, 85%. Anal. Calcd for $C_{42}H_{45}B_9N_1P_2Rh_1S_1 \cdot CH_2Cl_2$: C, 54.77; H, 5.02; N, 1.49; S, 3.40. Found: C, 54.42; H, 4.91; N, 1.17; S, 3.44 %. IR (ATR): ν 2568 vs (BH), 2492 vs (BH), 2456 vs (BH), 1259 m (BH), 1079 s, 1001 s, 797 m, 690 vs. ^{1}H NMR (300 MHz, CD_2Cl_2, 300 K): δ 8.89 (d, 2H, 2-CH_3-NC_5H_4), 8.07 (m, 1H, 2-CH_3-NC_5H_4), 7.72 (m, 2H, 2-CH_3-NC_5H_4), 7.50-7.00 (30H, $2PPh_3$), 3.04 (s, 3H, 2-CH_3-NC_5H_4). ^{31}P-{^{1}H} NMR (121 MHz, CD_2Cl_2, 300 K): δ +38.7 [d, $^1J_{RhP}$ = 149 Hz; $2PPh_3$]. LRMS (MALDI$^+$/DCTB): *m/z* 596 [M - $(PPh_3)]^+$. Isotope envelopes match those calculated from the known isotopic abundances of the constituent elements.

[1,1-$(PPh_3)_2$-3-(3-Me-NC_5H_4)-*closo*-1,2-$RhSB_9H_8$] (10). The reaction was carried out with 126 mg (0.480 mmol) of PPh_3 and 30 mg (0.048 mmol) of [1,1-$(PPh_3)(\eta^2$-$C_2H_4)$-3-(3-Me-NC_5H_4)-*closo*-1,2-$RhSB_9H_8$] (**14**), stirring for 12 h. Yield: 33 mg, 0.0385 mmol, 80%. Anal. Calcd for $C_{42}H_{45}B_9N_1P_2Rh_1S_1 \cdot CH_2Cl_2$: C, 54.77; H, 5.02; N, 1.49; S, 3.40. Found: C, 54.33; H, 4.94; N, 1.37; S, 3.34. IR (ATR): ν 2569 vs (BH), 2490 vs (BH), 2459 vs (BH), 1258 m (BH), 1081 s, 1003 s, 796 m, 691 vs. ^{1}H NMR (300 MHz, CD_2Cl_2, 300 K): δ 8.92 (d, 2H, 3-CH_3-NC_5H_4), 8.01 (m, 1H, 3-CH_3-NC_5H_4), 7.54 (m, 1H, 3-CH_3-NC_5H_4), 7.26-7.00 (30H, $2PPh_3$), 2.48 (s, 3H, 3-CH_3-NC_5H_4). ^{31}P-{^{1}H} NMR (121 MHz, CD_2Cl_2, 300 K): δ 40.2 [d, $^1J_{RhP}$ = 147 Hz; $2PPh_3$]. LRMS (MALDI$^+$/DCTB): *m/z*

596 [M - (PPh_3)]$^+$. Isotope envelopes match those calculated from the known isotopic abundances of the constituent elements.

[1,1-(PPh_3)$_2$-3-(4-Me-NC_5H_4)-*closo*-1,2-$RhSB_9H_8$] (11). The reaction was carried out with 105 mg (0.40 mmol) of PPh_3 and 25 mg (0.040 mmol) of [1,1-(PPh_3)(η^2-C_2H_4)-3-(4-Me-NC_5H_4)-*closo*-1,2-$RhSB_9H_8$] (**15**), stirring for 16 h. Yield: 26 mg, 0.030 mmol, 75%. Anal. Calcd for $C_{42}H_{45}B_9N_1P_2Rh_1S_1 \cdot 2CH_2Cl_2$: C, 51.41; H, 4.80; N, 1.36; S, 3.12 %. Found: C, 50.91; H, 4.35; N, 0.88; S, 2.64. IR (ATR): ν 2502 vs (BH), 2453 vs (BH), 1264 m (BH), 1085 s, 1004 s, 693 vs. ^{1}H NMR (300 MHz, CD_2Cl_2, 300 K): δ 8.75 (d, 2H, 4-CH_3-NC_5H_4), 7.51 (m, 2H, 4-CH_3-NC_5H_4), 7.25-7.03 (30H, 2PPh_3), 2.73 (s, 3H, 4-CH_3-NC_5H_4). ^{31}P-{^{1}H} NMR (121 MHz, CD_2Cl_2, 300 K): δ 39.6 [d, $^1J_{RhP}$ = 153 Hz; 2PPh_3]. LRMS (MALDI$^+$/DCTB): *m/z* 595 [M - (PPh_3) - H]$^+$. Isotope envelopes match those calculated from the known isotopic abundances of the constituent elements.

Ethylene-ligated *closo*-rhodathioboranes (13-15). As a general procedure, 100 mg of the corresponding hydridorhodathiaborane, [8,8,8-(PPh_3)$_2$H-9-(L)-*nido*-8,7-$RhSB_9H_9$], where L= 2-Me-NC_5H_4 (**3**), 3- Me-NC_5H_4 (**4**) or 4-Me-NC_5H_4 (**5**), was dissolved in 20 ml of CH_2Cl_2 in a Schlenk tube. After three freeze-thaw cycles, a balloon containing ethylene was attached to the Schlenk tube, and the rhodathiaborane solution exposed to the gas. The system was stirred at room temperature. After a variable length of time, the reaction mixture was concentrated by solvent evaporation under vacuum, and hexane was added to produce an orange-red precipitate, which was washed several times with hexane. The solid was crystallized from CH_2Cl_2/hexane to isolate the respective ethylene-ligated clusters, [1,1-(η^2-C_2H_4)(PPh_3)-3-(L)-*closo*-1,2-$RhSB_9H_8$].

[1,1-(PPh_3)(η^2-C_2H_4)-3-(2-Me-NC_5H_4)-*closo*-1,2-$RhSB_9H_8$] (13). The reaction was carried out with 100 mg (0.116 mmol) of **3**, and the solution was exposed to an ethylene atmosphere for 2 h. Yield: 62 mg, 0.099 mmol, 86%. Anal. Calcd for $C_{26}H_{34}B_9N_1P_1Rh_1S_1$: C, 50.06; H, 5.49; N, 2.5; S, 5.14. Found: C, 50.26; H, 5.63; N, 2.32; S, 5.01. IR (ATR): ν 2528 vs (BH), 2507 vs (BH), 2497 vs (BH), 2472 vs (BH), 2452 vs (BH), 1618 w, 1476 s, 1451 w, 1430 s, 1260 m, 1151 m, 1087 s, 1010 m, 946 m, 748 m,

692 s, 526 s, 492 m, 456 m (Rh-C_2H_4), 418 m (Rh-C_2H_4), 325 w (RhP). ^{1}H NMR (300 MHz, CD_2Cl_2, 300 K): δ 9.45 (m, 2H, 2-CH_3-NC_5H_5), 8.07 (m, 2H, 2-Me-NC_5H_5), 7.70-7.01 (15H, PPh_3), 3.05 (s, 3H, 2-CH_3-NC_5H_5), 2.16 (m, 2H, C_2H_4), 1.99 (m, 2H, C_2H_4). ^{31}P-{^{1}H} NMR (121 MHz, CD_2Cl_2, 300 K): δ 34.19 [d, $^1J_{RhP}$ = 134 Hz, PPh_3]. LRMS (MALDI$^+$/DCTB): *m/z* 595 [M - (C_2H_4) - H]$^+$. Isotope envelopes match those calculated from the known isotopic abundances of the constituent elements**.**

[1,1-(PPh_3)(η^2-C_2H_4)-3-(3-Me-NC_5H_4)-*closo*-1,2-$RhSB_9H_8$] (14). The reaction was carried out with 100 mg (0.116 mmol) of **4**, and the solution was exposed to an ethylene atmosphere for 4 h. Yield: 60 mg, 0.096 mmol, 83%. Anal. Calcd for $C_{26}H_{34}B_9N_1P_1Rh_1S_1$: C, 50.06; H, 5.49; N, 2.5; S, 5.14. Found: C, 50.46; H, 5.66; N, 2.30; S, 5.08.IR (ATR): *v* 2529 vs (BH), 2505 vs (BH), 2499 vs (BH), 2476 vs (BH), 2453 vs (BH), 1616 w, 1479 s, 1450 w, 1432 s, 1261 m, 1152 m, 1089 s, 1010 m, 947 m, 747 m, 692 s, 525 s, 491 m, 455 m (Rh-C_2H_4), 417 m (Rh-C_2H_4), 326 w (RhP). ^{1}H NMR (300 MHz, CD_2Cl_2, 300 K): δ 9.14 (m, 2H, 3-CH_3-NC_5H_4), 8.44 (m, 1H, 3-CH_3-NC_5H_4), 8.10 (m, 1H, 3-CH_3-NC_5H_4), 7.70-7.03 (15H, PPh_3), 2.52 (s, 3H, 3-CH_3-NC_5H_4), 2.28 (m, 2H,C_2H_4), 2.05 (m, 2H, C_2H_4). ^{31}P-{^{1}H} NMR (121 MHz, CD_2Cl_2, 300 K): δ 40.3 [d, $^1J_{RhP}$ = 137 Hz, PPh_3]. LRMS (MALDI$^+$/DCTB): *m/z* 595 [M - (C_2H_4) - H]$^+$. Isotope envelopes match those calculated from the known isotopic abundances of the constituent elements.

[1,1-(PPh_3)(η^2-C_2H_4)-3-(4-Me-NC_5H_4)-*closo*-1,2-$RhSB_9H_8$] (15). The reaction was carried out with 100 mg (0.116 mmol) of **5**, and the solution was exposed to an ethylene atmosphere for 12 h. Yield: 54 mg, 0.087 mmol, 75%. Anal. Calcd for $C_{26}H_{34}B_9N_1P_1Rh_1S_1 \cdot CH_2Cl_2$: C, 45.76; H, 5.12; N, 1.98; S, 4.52. Found: C, 45.91; H, 4.98; N, 1.69; S, 4.07. IR (ATR): *v* 2549 vs (BH), 2517 vs (BH), 2482 vs (BH), 2470 vs (BH), 1630 s, 1478 m, 1451 w, 1433 s, 1256 w, 1161 m, 1090 s, 1005 s, 936 m, 743 s, 693 vs, 525 vs, 491 s, 457 m (Rh-C_2H_4), 424 m (Rh-C_2H_4), 339 w (RhP). ^{1}H NMR (300 MHz, CD_2Cl_2, 300 K): δ 9.14 (m, 2H, 4-CH_3-NC_5H_4), 7.53 (m, 2H, 4-CH_3-NC_5H_4), 7.70-7.01 (15H, PPh_3), 2.71 (s, 3H, 4-CH_3-NC_5H_4), 2.26 (m, 2H, C_2H_4), 2.06 (m, 2H, C_2H_4). ^{31}P-{^{1}H} NMR (121 MHz, CD_2Cl_2, 300 K): δ 40.3 [d,

$^1J_{RhP}$ = 137 Hz, PPh_3]. LRMS (MALDI$^+$/DCTB) *m/z* 596 [M - (C_2H_4)]$^+$. Isotope envelopes match those calculated from the known isotopic abundances of the constituent elements.

CO-ligated *closo*-rhodathioboranes (17-19)

The procedure was the same as that for ethylene, but using a CO filled balloon.

[1,1-(PPh_3)(CO)-3-(2-Me-NC_5H_4)-*closo*-1,2-$RhSB_9H_8$] (17). The reaction was carried out with 60 mg (0.070 mmol) of **3** with stirring under an atmosphere of CO for 2 h. Yield: 37.6 mg, 0.0604 mmol, 87%. Anal. Calcd for $C_{25}H_{30}B_9N_1O_1P_1Rh_1S_1 \cdot CH_2Cl_2$: C, 44.06; H, 4.55; N, 1.98; S, 4.52. Found: C, 44.09; H, 4.53; N, 1.83; S, 4.27. IR (ATR): *ν* 2567 vs (BH), 2520 vs (BH), 2493 vs (BH), 2466 vs (BH), 1982 vs (CO), 1632 m, 1479 m, 1434 m, 1262 m, 1161 m, 1092 m, 1006 m, 935 m, 935 m, 877 m, 829 m, 800 m, 746 m, 692 vs, 577 w, 525 vs. ^{1}H NMR (300 MHz, CD_2Cl_2, 300 K): *δ* 9.41 (d, 1H, 2-CH_3-NC_5H_4), 8.04 (d, 1H, 2-CH_3-NC_5H_4), 7.62 (t, 2H, 2-CH_3-NC_5H_4), 7.50-7.05 (15H, PPh_3), 3.02 (m, 3H, 2-CH_3-NC_5H_4). ^{31}P-{^{1}H} NMR (121 MHz, CD_2Cl_2, 300 K): *δ* 37.7 (d, $^1J_{RhP}$ = 133 Hz; PPh_3). LRMS (MALDI$^+$/DCTB): *m/z* 596 [M - (CO)]$^+$. Isotope envelopes match those calculated from the known isotopic abundances of the constituent elements.

[1,1-(PPh_3)(CO)-3-(3-Me-NC_5H_4)-*closo*-1,2-$RhSB_9H_8$] (18). The reaction was carried out with 150 mg (0.174 mmol) of **4** and the stirring under an atmosphere of CO was maintained for 2 h. Yield: 97.0 mg, 0.156 mmol, 90%. Anal. Calcd for $C_{25}H_{30}B_9N_1O_1P_1Rh_1S_1 \cdot CH_2Cl_2$: C, 44.06; H, 4.55; N, 1.98; S, 4.52. Found: C, 44.41; H, 4.42; N, 1.76; S, 4.32. IR (ATR): *ν* 2563 vs (BH), 2519 vs (BH), 2494 vs (BH), 2464 vs (BH), 1974 vs (CO), 1619 m, 1478 m, 1433 m, 1180 m, 1093 m, 1005 m, 939 m, 742 m, 684 vs, 524 v. ^{1}H NMR (300 MHz, CD_2Cl_2, 300 K): *δ* 8.90 (d, 2H, 3-CH_3-NC_5H_4), 8.01 (d, 1H, 3-CH_3-NC_5H_4), 7.58 (t, 1H, 3-CH_3-NC_5H_4), 7.34-7.28 (15H, PPh_3), 2.40 (m, 3H, 3-CH_3-NC_5H_4). ^{31}P-{^{1}H} NMR (121 MHz, CD_2Cl_2, 300 K): *δ* 37.9 (d, $^1J_{RhP}$ = 136 Hz; PPh_3). LRMS (MALDI$^+$/DCTB): *m/z* 596 [M - (CO)]$^+$. Isotope envelopes match those calculated from the known isotopic abundances of the constituent elements.

[1,1-(PPh_3)(CO)-3-(4-Me-NC_5H_4)-*closo*-1,2-$RhSB_9H_8$] (19). The reaction was carried out with 30 mg (0.035 mmol) of **5** and the stirring under an atmosphere of CO was maintained for 8 h. Yield: 20.0 mg, 0.032 mmol, 91 %. Anal. Calcd for $C_{25}H_{30}B_9N_1O_1P_1Rh_1S_1 \cdot CH_2Cl_2$: C, 44.06; H, 4.55; N, 1.98; S, 4.52 %. Found: C, 44.51; H, 4.43; N, 1.73; S, 4.02 %. IR (ATR): ν 2567 vs (BH), 2523 vs (BH), 2501 vs (BH), 2465 vs (BH), 1993 vs (CO), 1978 vs (CO), 1632 m, 1479 m, 1452 w, 1434 m, 1163 m, 1092 s, 1006 m, 935 m, 746 s, 692 vs, 525 vs. ^{1}H NMR (300 MHz, CD_2Cl_2, 300 K): δ 8.97 (m, 2H, 4-CH_3-NC_5H_4), 7.46 (m, 2H, 4-CH_3-NC_5H_4), 7.36-7.27 (15H, PPh_3), 2.65 (s, 3H, 4-CH_3-NC_5H_4). ^{31}P-{^{1}H} NMR (121 MHz, CD_2Cl_2, 300 K): δ 37.9 (d, $^1J_{RhP}$ = 132 Hz; PPh_3). LRMS (MALDI$^+$/DCTB): *m/z* 596 [M - (CO)]$^+$. Isotope envelopes match those calculated from the known isotopic abundances of the constituent elements.

Reactions with carbon monoxide: characterization of intermediates

Carbon monoxide was bubbled for several minutes (3 to 9) through a CD_2Cl_2 solution of the corresponding *nido*-hydridorhodathiaborane, **2-5**, in a 5 mm NMR tube at room temperature. The sample was subsequently cooled to -50 ºC in an isopropanol bath, and transferred to an NMR spectrometer in which the temperature of the probe was set to -50 ºC. The system was studied at different temperatures, allowing the identification of the different intermediates that form before hydrogen loss occurs to yield the above described CO-ligated *closo*-clusters, **16-19**. The following are the NMR data for the reaction mixtures that contain the labile new species. Spectra can be seen in the main text as well the supplementary material of this paper.

Reaction of 2 with CO: 9 minutes of CO bubbling. ^{1}H-{^{11}B} NMR (500 MHz, CD_2Cl_2, 223 K): δ +9.27 to +7.06 (aromatics, NC_5H_5, PPh_3), +3.92 (s, BH), +3.41 (s, BH), +1.86 (s, BH), +0.28 (s, BH), -1.66 (low intensity br s, BH), -2.93 (s, BHB), -4.56 (s, BHB), -10.96 (low intensity apparent t, $^1J_{RhH}$ = 20.4 Hz, RhH), -11.25 (d, $^1J_{RhH}$ = 22.1 Hz, 1H). There are also resonances corresponding to **2**, which is in solution as a minor species. ^{31}P-{^{1}H} NMR (202 MHz, CD_2Cl_2, 203 K): δ +38.9 (d, $^1J_{RhP}$ = 131 Hz, compound **16**), +36.6 (d, $^1J_{RhP}$ = 125.2 Hz), +35.2 (d, $^1J_{RhP}$ = 99.4 Hz), +29.5 (d, $^1J_{RhP}$ = 121.9 Hz),

+28.6 ($O=PPh_3$), -7.9 (PPh_3): the resonances exhibit a 1:2.94:11.30:1.60:0.77:14.04 relative intensity ratio, respectively. [^{1}H-^{31}P]-HMBC (500 MHz, CD_2Cl_2, 203 K) {ordered as (δ_H, δ_P) correlation}: (-10.96, +29.5), (-11.35, +35.2); as expected, all the ^{31}P resonances exhibit correlations with aromatic signals.

Reaction of 3 with CO: 3 minutes of CO bubbling. ^{11}B-{^{1}H} NMR (160 MHz; CD_2Cl_2, 273 K): δ +12.8 (s, minor species) +8.2 (d, $^1J_{BH}$ = 118 Hz, major species), +5.8 (minor species), +3.6 (d, $^1J_{BH}$ = 72 Hz, major), -2.1 (minor species), -4.4 (minor species), -9.2 (d, $^1J_{BH}$ = 137 Hz, minor species), -13.5 (major species), -12.5 (minor species), -13.5 (major species), -18.5 (minor species), -19.6 (d, $^1J_{BH}$ = 127 Hz, major species), -22.3 (d, $^1J_{BH}$ = 146 Hz, major species), -24.6 (major species), -26.0 (d, $^1J_{BH}$ = 146 Hz, major species), -28.3 (d, $^1J_{BH}$ = 145 Hz, minor species), -32.1 (minor species). ^{1}H-{^{11}B} NMR (400 MHz, CD_2Cl_2, 223 K): δ +9.21 (d, 5.2 Hz, o-2-Me-NC_5H_4, minor species), +9.15 (d, 5.5 Hz, o-2-Me-NC_5H_4, major species), +7.98 (*pseudo*-t, 7.5 Hz, 2-Me-NC_5H_4, major species), +7.92 (*pseudo*-t, 7.5 Hz, 2-Me-NC_5H_4, minor species), +7.57 to +7.16 (aromatics, 2-Me-NC_5H_4, PPh_3), +4.04 (BH, minor species), +3.37 (BH, major species), +3.03 (BH, major), +2.92 (s, CH_3; minor species), +2.60 (BH, minor species), +2.35 (BH, major species), +2.26 (s, CH_3; major species), +2.18 (BH, major species), +2.04 (BH, minor species), +1.87 (BH, major species), +1.32 (2BH, major species), +0.90 (BH, minor species), +0.15 (BH, major species), -2.88 (s, BHB), -4.63 (s, BHB), -11.33 (d, $^1J_{RhH}$ = 22.3 Hz, RhH). ^{1}H-{^{11}B} NMR (400 MHz, CD_2Cl_2, 273 K): selected resonances, -2.81 (s, BHB), -4.59 (s, BHB), -11.42 (d, $^1J_{RhH}$ = 17.8 Hz, RhH), relative intensity ratio 1:1:0.27. ^{31}P-{^{1}H} NMR (162 MHz, CD_2Cl_2, 223 K): δ +35.5 (d, $^1J_{RhP}$ = 127 Hz), +35.0 (br. d, $^1J_{RhP}$ = 91 Hz; this broad signal overlaps partially with the previous resonance), +28.4 ($O=PPh_3$), -7.4 (PPh_3): the resonances exhibit a 2.0:0.7:0.4:2.3 relative intensity ratio, respectively. [^{1}H-^{31}P]-HMBC (500 MHz, CD_2Cl_2, 203 K) {ordered as (δ_H, δ_P) correlation}: [-11.28, +35.7 (br. peak)]. [^{1}H-^{1}H]-NOESY (500 MHz, CD_2Cl_2, 273 K): (-2.75, -11.31), this off diagonal peak is of the same phase as the diagonal peaks, demonstrating that the correlation is

due to chemical exchange between the Rh–H hydride ligand and the B–H–B bridging hydrogen atom of one of the intermediates.

Reaction of 4 with CO: ^{1}H-{^{11}B} NMR (400 MHz, CD_2Cl_2, 223 K): δ +8.97 (m, 3-Me-NC_5H_4, minor), +8.88 (m, 3-Me-NC_5H_4, major), +8.75 (s, 3-Me-NC_5H_4, major), +8.65 (s, 3-Me-NC_5H_4, major), +7.65 to +6.71 (aromatics, 4-Me-NC_5H_4 and PPh_3), +3.95 (s, BH, major), +3.50 (s, BH, major), +2.99 (s, BH, minor), +2.11 (s, CH_3), +1.99 (s, BH, major), +1.39 (s, BH, major), +1.29 (s, BH), +1.05 (s, BH), +0.89 (s, BH), +0.24 (s, BH), -1.60 (BH, minor species), -2.99 (s, BHB), -4.55 (s, BHB), -10.88 (low intensity apparent t, J = 10.88 Hz, RhH), -11.86 (d, $^{1}J_{RhH}$ = 22.6 Hz, RhH).

Reaction of 5 with CO: ^{11}B-{^{1}H} NMR (160 MHz; CD_2Cl_2, 273 K): δ +55.2 (compound **19**), +27.9 (compound **19**), +15.9, +8.17, +7.0, +5.0 ($^{1}J_{BH}$ = 119 Hz), +1.2, -3.1, -9.8 ($^{1}J_{BH}$ = 145 Hz), -13.5, -19.3, -20.3, -22.8 (compound **19**), -25.2 ($^{1}J_{BH}$ = 132 Hz), -28.2 ($^{1}J_{BH}$ = 145 Hz), -32.5 (compound **19**). ^{1}H-{^{11}B} NMR (500 MHz, CD_2Cl_2, 223 K): δ +8.84 (br. m, 4-Me-NC_5H_4), +8.67 (d, J = 6.0 Hz, 4-Me-NC_5H_4), +7.65 to +6.71 (aromatics, 4-Me-NC_5H_4 and PPh_3), +3.90 (s,BH), +3.39 (s, BH), +2.57 (s, BH), +2.11 (s, CH_3), +1.96 (s, BH), +1.37 (s, BH), +1.29 (s, BH), +1.05 (s, BH), +0.89 (s, BH), +0.24 (s, BH), -1.64 (BH, minor species), -2.99 (s, BHB), -4.55 (s, BHB), -10.95 (low intensity apparent t, J = 19.9 Hz, RhH), -11.26 (d, $^{1}J_{RhH}$ = 22.6 Hz, RhH). ^{1}H-{^{11}B} NMR (500 MHz, CD_2Cl_2, 300 K): δ +9.18 to +6.38 (aromatics, 4-Me-NC_5H_4 and PPh_3), +3.82 (BH), +3.40 (BH), +3.04 (BH), +2.65 (BH), +2.51 (s, CH_3; major component), +2.30 (BH), +2.24 (BH), +2.11 (s, CH_3; minor component), +1.45 (BH), +1.28 (BH), +1.02 (BH), +0.21 (BH), -2.92 (v. broad, BHB), -4.51 (v. broad, BHB), -10.96 (apparent triplet, J_{RhH} = 22.9 Hz, minor species), -11.35 (d, $^{1}J_{RhH}$ = 21.3 Hz, RhH); there are also resonances corresponding to **19**, which is in solution as a minor species. ^{31}P-{^{1}H} NMR (121 MHz, CD_2Cl_2, 223 K): δ +38.6 (d, $^{1}J_{RhP}$ = 131 Hz, compound **19**), +36.6 (d, $^{1}J_{RhP}$ = 125 Hz), +34.5 (d, $^{1}J_{RhP}$ = 103 Hz), +29.8 (d, $^{1}J_{RhP}$ = 122 Hz), +28.4 (O=PPh_3), -7.4 (free PPh_3): the resonances exhibit a 1.00:1.90:9.86:0.76:0.28:11.50 relative intensity ratio, respectively. ^{31}P-{^{1}H} NMR (121 MHz, CD_2Cl_2, 300 K): δ +37.8 (d, $^{1}J_{RhP}$ = 126 Hz, compound **19**) +35.8 (very broad, PPh_3), +32.8 (very broad, PPh_3),

+27.2 ($O=PPh_3$), -5.3 (free PPh_3): the resonances exhibit a 1.00:0.24:0.33:0.04:1.02 relative intensity ratio, respectively. [^{1}H-^{31}P]-HMBC (500 MHz, CD_2Cl_2, 223 K) {ordered as (δ_H, δ_P) correlation}: (-10.95, +29.8), (-11.35, +34.5), (+2.65, +34.5); as expected, all the ^{31}P resonances correlate with aromatic signals.

Reactions with alkenes

[**8,8,8-H(PPh$_3$)$_2$-9-(NC$_5$H$_5$)-*nido*-8,7-RHSB$_9$H$_9$] (2) with cyclohexene.** 2 mg (0.0025 mmol) of **2** and a 20-fold excess of cyclohexane were stirred for 7 days with no sign of reaction.

[**8,8,8-H(PPh$_3$)$_2$-9-(NC$_5$H$_5$)-*nido*-8,7-RHSB$_9$H$_9$] (2) with 1-hexene.** In a 5 mm NMR tube, 2 mg (0.0025 mmol) of **2** was dissolved in 0.6 mL of CH_2Cl_2 together with a 20-fold excess of 1-hexene. GC after one day of reaction showed a mixture of 1-hexene (75%), 2-hexene (17%), 3-hexene (7%) and hexane (1%).

[**8,8,8-H(PPh$_3$)$_2$-9-(NC$_5$H$_5$)-*nido*-8,7-RHSB$_9$H$_9$] (2) with propylene.** In a 5 mm NMR tube, 16 mg (0.018 mmol) of **2** was dissolved in 0.6 mL of CD_2Cl_2 in a NMR tube and propylene was bubbled through the solution for 5 minutes. After four days of stirring, the composition of the reaction mixture contained propylene, some propane, *closo*-derivative, **8** (65%) and starting material, **2** (35%).

[**8,8,8-H(PPh$_3$)$_2$-9-(2-Me-NC$_5$H$_4$)-*nido*-8,7-RHSB$_9$H$_9$] (3) with cyclohexene.** In a 5 mm NMR tube, 12.5 mg (0.014 mmol) of **3** in 0.6 mL of CD_2Cl_2 and a 20-fold excess of cyclohexene were dissolved. After 5 days, there was formation of cyclohexane (2%) and the *closo*-rhodathiaborane, **9**.

[**8,8,8-H(PPh$_3$)$_2$-9-(2-Me-NC$_5$H$_4$)-*nido*-8,7-RHSB$_9$H$_9$] (3) with 1-hexene.** In a Schlenk tube, 12.5 mg (0.014 mmol) of **3** was dissolved in 0.6 mL of CH_2Cl_2 with a 20-fold excess of 1-hexene. The solution was stirred at room temperature under an atmosphere of argon. The reaction was monitored by GC, and after one day the composition of the mixture was 34 % of 2-hexene, 63% of 1-hexene and 3% of hexane. Compound **3** afforded the *closo*-derivative **9**.

[**8,8,8-H(PPh$_3$)$_2$-9-(2-Me-NC$_5$H$_4$)-*nido*-8,7-RHSB$_9$H$_9$] (3) with propylene.** In an NMR tube, 14 mg (0.016 mmol) of **3** was dissolved in 0.6 mL of CD_2Cl_2 and propylene gas was bubbled through the

solution for 5 minutes. In 1 hour, the hydridorhodathiaborane underwent transformation to the *closo*-cluster, **9**, with concomitant formation of propane.

ACKNOWLEDGMENT . We acknowledge the Spanish Ministry of Science and Innovation (CTQ2009-10132, CONSOLIDER INGENIO, CSD2009-00050, MULTICAT and CSD2006-0015, Crystallization Factory) for support of this work. B.C. thanks the "Diputación General de Aragón" for a pre-doctoral scholarship. We want also thank Dr J. Bould for useful discussions.

REFERENCES

(1) (a) Grimes, R. N. In *Comprehensive Organometallic Chemistry*; Wilkinson, G., Stone, F. G. A., Abel, E. W., Eds.; Pergamon Press Ltd.: Oxford, 1982; Vol. 1. (b) Grimes, R. In *Metal Interactions with Boron Clusters*; Grimes, R., Ed.; Springer US, 1982. (c) Grimes, R. N. *Chem. Rev.* **1992**, *92*, 251. (d) Grimes, R. N. In *Comprehensive Organometallic Chemistry II*; Abel, E. W., Stone, F. G. A., Wilkinson, G., Eds.; Pergamon: Oxford, 1995; Vol. 1. (e) McGrath, T. D.; Stone, F. G. A. In *Advances in Organometallic Chemistry, Vol 53*, 2005; Vol. 53. (f) Hodson, B. E.; McGrath, T. D.; Stone, F. G. A. *Organometallics* **2005**, *24*, 1638. (g) McGrath, T. D.; Stone, F. G. A. *J. Organomet. Chem.* **2004**, *689*, 3891. (h) Ellis, D. D.; Jelliss, P. A.; Stone, F. G. A. *Spec. Publ. - R. Soc. Chem.* **2000**, *253*, 291. (i) Jelliss, P. A.; Stone, F. G. A. *J. Organomet. Chem.* **1995**, *500*, 307. (j) Brew, S. A.; Stone, F. G. A. *Adv. Organomet. Chem.* **1993**, *35*, 135. (k) Stone, F. G. A. *Adv. Organomet. Chem.* **1990**, *31*, 53. (l) Saxena, A. K.; Maguire, J. A.; Hosmane, N. S. *Chem. Rev.* **1997**, *97*, 2421. (m) Saxena, A. K.; Hosmane, N. S. *Chem. Rev.* **1993**, *93*, 1081.

(2) (a) Kennedy, J. D. *Prog. Inorg. Chem.* **1986**, *34*, 211. (b) Kennedy, J. D. *Prog. Inorg. Chem.* **1984**, *32*, 519. (c) Barton, L., Strivastava, D. K. In *Comprehensive Organometallic Chemistry II*; Abel, E. W., Stone, F. G. A., Wilkinson, G., Ed.; Pergamon: New York, 1995; Vol. 1. (d) Todd, L. T. In *Comprehensive Organometallic Chemistry II*; Abel, E. W., Stone, F. G. A., Wilkinson, G., Eds.; Elsevier Science: Oxford, 1995; Vol. 1. (e) Todd, L. T. In *Comprehensive*

Organometallic Chemistry; Wilkinson, G., Stone, F. G. A., Abel, E. W., Eds.; Pergamon Press Ltd.: Oxford, 1982; Vol. 1. (f) Wesemann, L. In *Comprehensive Organometallic Chemistry*; Mingos, D. M. P., Crabtree, R. H., Eds.; Elsevier: Oxford, 2007; Vol. 3. (g) Weller, A. S. In *Comprehensive Organometallic Chemistry III*; Crabtree, R. H., Mingos, D. M. P., Eds.; Elsevier: Oxford, 2007; Vol. 3.

(3) (a) Wade, K. *Adv. Inorg. Chem. Radiochem.* **1976**, *18*, 1. (b) Williams, R. E. *Adv. Inorg. Chem. Radiochem.* **1976**, *18*, 67.

(4) Ferguson, G.; Jennings, M. C.; Lough, A. J.; Coughlan, S.; Spalding, T. R.; Kennedy, J. D.; Fontaine, X. L. R.; Stibr, B. *J. Chem. Soc., Chem. Commun.* **1990**, 891.

(5) Calvo, B.; Kess, M.; Macias, R.; Cunchillos, C.; Lahoz, F. J.; Kennedy, J. D.; Oro, L. A. *Dalton Trans.* **2011**, *40*, 6555.

(6) (a) Álvarez, Á.; Macías, R.; Fabra, M. J.; Lahoz, F. J.; Oro, L. A. *J. Am. Chem. Soc.* **2008**, *130*, 2148. (b) Álvarez, Á.; Macías, R.; Bould, J.; Fabra, M. J.; Lahoz, F. J.; Oro, L. A. *J. Am. Chem. Soc.* **2008**, *130*, 11455.

(7) Calvo, B.; Macias, R.; Polo, V.; Artigas, M. J.; Lahoz, F. J.; Oro, L. A. *Chem. Commun.* **2013**, *49*, 9863.

(8) Calvo, B.; Macias, R.; Artigas, M. J.; Lahoz, F. J.; Oro, L. A. *Dalton Trans.* **2014**, *43*, 5121.

(9) Calvo, B.; Álvarez, Á.; Macías, R.; García-Orduña, P.; Lahoz, F. J.; Oro, L. A. *Organometallics* **2012**, *31*, 2986.

(10) Álvarez, Á.; Macías, R.; Bould, J.; Cunchillos, C.; Lahoz, F. J.; Oro, L. A. *Chem. Eur. J.* **2009**, *15*, 5428.

(11) Calvo, B.; Macías, R.; Artigas, M. J.; Lahoz, F. J.; Oro, L. A. *Chem. Eur. J.* **2013**, *19*, 3905.

(12) Calvo, B.; Macías, R.; Artigas, M. J.; Lahoz, F. J.; Oro, L. A. *Inorg. Chem.* **2012**, *52*, 211.

(13) (a) Macías, R.; Bould, J.; Holub, J.; Kennedy, J. D.; Štibr, B.; Thornton-Pett, M. *Dalton Trans.* **2007**, 2885 . (b) Bould, J.; Macías, R. *J. Organomet. Chem.* **2014**, *761*, 120.

(14) McAnaw, A.; Scott, G.; Elrick, L.; Rosair, G. M.; Welch, A. J. *Dalton Trans.* **2013**, *42*, 645.

(15) (a) Macías, R.; Holub, J.; Kennedy, J. D.; Stibr, B.; Thornton-Pett, M. *J. Chem. Soc., Chem. Comm.* **1994**, 2265. (b) Nestor, K.; Kennedy, J. D.; Thornton-Pett, M.; Holub, J.; Stibr, B. *Inorg. Chem.* **1992**, *31*, 3339. (c) Bould, J.; Rath, N. P.; Barton, L. *Organometallics* **1996**, *15*, 4916.

(16) Bould, J.; Cunchillos, C.; Lahoz, F. J.; Oro, L. A.; Kennedy, J. D.; Macías, R. *Inorg. Chem.* **2010**, *49*, 7353.

(17) Beall, H.; Bushweller, C. H.; Dewkett, W. J.; Grace, M. *J. Am. Chem. Soc.* **1970**, *92*, 3484.

(18) Merrick, J. P.; Moran, D.; Radom, L. *J. Phys. Chem. A* **2007**, *111*, 11683.

(19) Kononova, E. G.; Leites, L. A.; Bukalov, S. S.; Pisareva, I. V.; Chizhevsky, I. T.; Kennedy, J. D.; Bould, J. *Eur. J. Inorg. Chem.* **2007**, *2007*, 4911.

(20) (a) Nestor, K.; Fontaine, X. L. R.; Greenwood, N. N.; Kennedy, J. D.; Plešek, J.; Štíbr, B.; Thornton-Pett, M. *Inorg. Chem.* **1989**, *28*, 2219. (b) Bown, M.; Fontaine, X. L. R.; Greenwood, N. N.; Kennedy, J. D.; Thornton-Pett, M. *Organometallics* **1987**, *6*, 2254. (c) Nestor, K.; Fontaine, X. L. R.; Greenwood, N. N.; Kennedy, J. D.; Thornton-Pett, M. *J. Chem. Soc., Chem. Commun.* **1989**, 455.

(21) Volkov, O.; Radacki, K.; Thomas, R. L.; Rath, N. P.; Barton, L. *J. Organomet. Chem.* **2005**, *690*, 2736.

(22) Balagurova, E. V.; Cheredilin, D. N.; Kolomnikova, G. D.; Tok, O. L.; Dolgushin, F. M.; Yanovsky, A. I.; Chizhevsky, I. T. *J. Am. Chem. Soc.* **2007**, *129*, 3745.

(23) (a) Long, J. A.; Marder, T. B.; Behnken, P. E.; Hawthorne, M. F. *J. Am. Chem. Soc.* **1984**, *106*, 2979. (b) Ellis, D. D. F., A.; Jelliss, P. A.; Kautz, J. A.; Stone, F. G. A.; Yu, P.-Y. *J. Chem. Soc., Dalton Trans.* **2000**, 2509. (c) Pisareva, I. V.; Konoplev, V. E.; Petrovskii, P. V.; Vorontsov, E. V.; Dolgushin, F. M.; Yanovsky, A. I.; Chizhevsky, I. T. *Inorg. Chem.* **2004**, *43*, 6228.

(24) (a) Hawthorne, M. F.; Ramachandran, B. M.; Kennedy, R. D.; Knobler, C. B. *Pure Appl. Chem.* **2006**, *78*, 1299. (b) Oconnell, D.; Patterson, J. C.; Spalding, T. R.; Ferguson, G.; Gallagher, J. F.; Li, Y. W.; Kennedy, J. D.; Macías, R.; Thornton-Pett, M.; Holub, J. *J. Chem. Soc., Dalton*

Trans. **1996**, 3323. (c) Macias, R.; Thornton-Pett, M.; Holub, J.; Spalding, T. R.; Faridoon, Y.; Stibr, B.; Kennedy, J. D. *J. Organomet. Chem.* **2008**, *693*, 435.

(25) Fontaine, X. L. R.; Kennedy, J. D. *J. Chem. Soc., Dalton Trans.* **1987**, 1573.

(26) Keeler, J. *Understanding NMR Spectroscopy*; John Wiley & Sons, Ltd, 2010.

(27) Henderson, W.; McIndoe, J. S. *Mass Spectrometry of Inorganic and Organometallic Compounds*; 2005 ed.; John Wiley & Sons Ltd., 2005.

(28) Otwinowski, Z.; Minor, W. In *Methods Enzymol.*; Carter, J. R. M. S. C. W., Ed.; Academic Press: New York, 1997; Vol. 276.

(29) Blessing, R. H. *Acta Cryst.* **1995**, *A51*, 33.

(30) Sheldrick, G. M. University of Göttingen: Göttingen, Germany, 1997.

(31) Sheldrick, G. M. *Acta Cryst.* **2008**, *A64*, 112.

(32) M. J. Frisch; G. W. Trucks; H. B. Schlegel; G. E. Scuseria; M. A. Robb; J. R. Cheeseman; G. Scalmani; V. Barone; B. Mennucci; G. A. Petersson; H. Nakatsuji; M. Caricato; X. Li; H. P. Hratchian; A. F. Izmaylov; J. Bloino; G. Zheng; J. L. Sonnenberg; M. Hada; M. Ehara; K. Toyota; R. Fukuda; J. Hasegawa; M. Ishida; T. Nakajima; Y. Honda; O. Kitao; H. Nakai; T. Vreven; J. A. Montgomery; Jr., J. E. P.; F. Ogliaro; M. Bearpark; J. J. Heyd; E. Brothers; K. N. Kudin; V. N. Staroverov; R. Kobayashi; J. Normand; K. Raghavachari; A. Rendell; J. C. Burant; S. S. Iyengar; J. Tomasi; M. Cossi; N. Rega; J. M. Millam; M. Klene; J. E. Knox; J. B. Cross; V. Bakken; C. Adamo; J. Jaramillo; R. Gomperts; R. E. Stratmann; O. Yazyev; A. J. Austin; R. Cammi; C. Pomelli; J. W. Ochterski; R. L. Martin; K. Morokuma; V. G. Zakrzewski; G. A. Voth; P. Salvador; J. J. Dannenberg; S. Dapprich; A. D. Daniels; Ö. Farkas; J. B. Foresman; J. V. Ortiz; J. Cioslowski; Fox, D. J.; Gaussian, Inc.: Wallingford CT, 2009.